Article

Cell Reports

Light Entrains Diurnal Changes in Insulin Sensitivity of Skeletal Muscle via Ventromedial Hypothalamic Neurons

Graphical Abstract

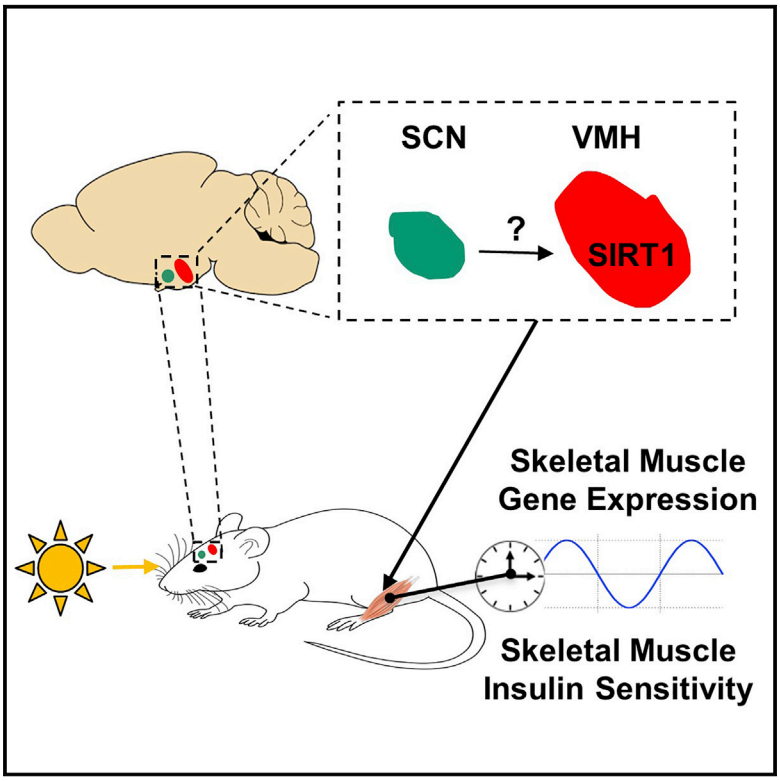

Highlights

- Response to insulin of metabolically relevant tissues varies in a diurnal fashion
- SF1 neurons govern diurnal variation in responsiveness to insulin in skeletal muscle
- Light inputs entrain diurnal variation in responsiveness to insulin in skeletal muscle
- Photic gain- or loss-of-function causes insulin resistance in skeletal muscle

Authors

Ebru Aras, Giorgio Ramadori, Kenichiro Kinouchi, ..., Pierre Baldi, Paolo Sassone-Corsi, Roberto Coppari

Correspondence

giorgio.ramadori@unige.ch (G.R.), roberto.coppari@unige.ch (R.C.)

In Brief

Aras et al. provide *in vivo* evidence that tissue responsiveness to insulin varies in a diurnal fashion. In skeletal muscle, the authors show that photic inputs entrain diurnal changes in clock genes expression and insulin sensitivity via SIRT1 in neurons within the hypothalamic ventromedial nucleus.

Aras et al., 2019, Cell Reports *27*, 2385–2398
May 21, 2019
https://doi.org/10.1016/j.celrep.2019.04.093

CellPress

Cell Reports
Article

Light Entrains Diurnal Changes in Insulin Sensitivity of Skeletal Muscle via Ventromedial Hypothalamic Neurons

Ebru Aras,[1,2,6] Giorgio Ramadori,[1,2,6,*] Kenichiro Kinouchi,[3] Yu Liu,[4] Rafael M. Ioris,[1,2] Xavier Brenachot,[1,2] Sanda Ljubicic,[1,2] Christelle Veyrat-Durebex,[1,2] Silvia Mannucci,[5] Mirco Galié,[5] Pierre Baldi,[4] Paolo Sassone-Corsi,[3] and Roberto Coppari[1,2,3,7,*]

[1]Diabetes Center of the Faculty of Medicine, University of Geneva, 1211 Geneva 4, Switzerland
[2]Department of Cell Physiology and Metabolism, Faculty of Medicine, University of Geneva, 1211 Geneva 4, Switzerland
[3]Center for Epigenetics and Metabolism, University of California, Irvine, Irvine, CA 92607, USA
[4]Institute for Genomics and Bioinformatics, School of Information and Computer Sciences, University of California Irvine, Irvine, CA 92697, USA
[5]Department of Neuroscience, Biomedicine and Movement, University of Verona, Piazzale L.A. Scuro 10, Verona 37134, Italy
[6]These authors contributed equally
[7]Lead Contact
*Correspondence: giorgio.ramadori@unige.ch (G.R.), roberto.coppari@unige.ch (R.C.)
https://doi.org/10.1016/j.celrep.2019.04.093

SUMMARY

Loss of synchrony between geophysical time and insulin action predisposes to metabolic diseases. Yet the brain and peripheral pathways linking proper insulin effect to diurnal changes in light-dark and feeding-fasting inputs are poorly understood. Here, we show that the insulin sensitivity of several metabolically relevant tissues fluctuates during the 24 h period. For example, in mice, the insulin sensitivity of skeletal muscle, liver, and adipose tissue is lowest during the light period. Mechanistically, by performing loss- and gain-of-light-action and food-restriction experiments, we demonstrate that SIRT1 in steroidogenic factor 1 (SF1) neurons of the ventromedial hypothalamic nucleus (VMH) convey photic inputs to entrain the biochemical and metabolic action of insulin in skeletal muscle. These findings uncover a critical light-SF1-neuron-skeletal-muscle axis that acts to finely tune diurnal changes in insulin sensitivity and reveal a light regulatory mechanism of skeletal muscle function.

INTRODUCTION

The balance between hormonal secretion and action is key for maintaining organismal homeostasis (Bass and Takahashi, 2010; Coppari et al., 2009; Vianna and Coppari, 2011). Secretion of several hormones (e.g., insulin) varies during the 24 h period (Czech, 2017; Gamble et al., 2014), and altered synchronization between geophysical time and hormonal action predisposes to metabolic diseases (e.g., diabetes) (Buxton et al., 2012; Masri and Sassone-Corsi, 2013; Scheer et al., 2009). Yet whether the responsiveness of hormones' target tissues also fluctuates around the clock and the mechanism(s) underlying this effect are poorly understood. In principle, a combination between abundance and appropriate tissues responsiveness could guarantee that the correct hormonal effect is achieved at the precise time and that metabolic homeostasis is preserved.

Diurnal changes in hormonal (as well as mRNA, protein, and metabolite) levels are synchronized to external inputs: zeitgeber times (ZTs) or time givers (e.g., light-dark and feeding-fasting cycles) (Asher and Sassone-Corsi, 2015; Eckel-Mahan et al., 2012; Yang et al., 2006). For example, insulin links carbohydrate and lipid metabolism to nutrient intake (Brenachot et al., 2017), and its circulating level varies during the 24 h period (Czech, 2017). Another hormone, melatonin, which is best known as a regulator of daily rhythms, has been suggested to influence insulin secretion and glucose balance (Garaulet et al., 2015; Rubio-Sastre et al., 2014). Tissue diurnal rhythms have been suggested to influence insulin signaling as altered core-clock gene expression (in either a whole-body or a tissue-specific manner) causes insulin resistance (Carrasco-Benso et al., 2016; Dyar et al., 2013; Marcheva et al., 2010; McDearmon et al., 2006; Paschos et al., 2012; Shi et al., 2013). Clinically, the rate of blood glucose decline after an intravenous glucose or insulin administration is highest in the morning compared with the afternoon (Carroll and Nestel, 1973; Gibson and Jarrett, 1972; Service et al., 1983; Van Cauter et al., 1991; Whichelow et al., 1974). In addition, exposure to photic input at the wrong time negatively affects glucose metabolism (Cheung et al., 2016; Opperhuizen et al., 2017; Versteeg et al., 2017). Together, these results suggest that responsiveness of target organs to insulin might vary around the clock and be influenced by changes in photic inputs. Nevertheless, whether tissue insulin sensitivity of key metabolic tissues fluctuates across the 24 h cycle and/or is affected by light inputs is unknown. Understanding these mechanisms will provide novel insights into mammalian physiology and be of great medical importance. For example, insulin resistance or severe hypoinsulinemia causes diabetes, a condition affecting about 450 million people worldwide (Anderson et al., 2015; Coppari and Bjørbæk, 2012). Many of these patients require daily insulin

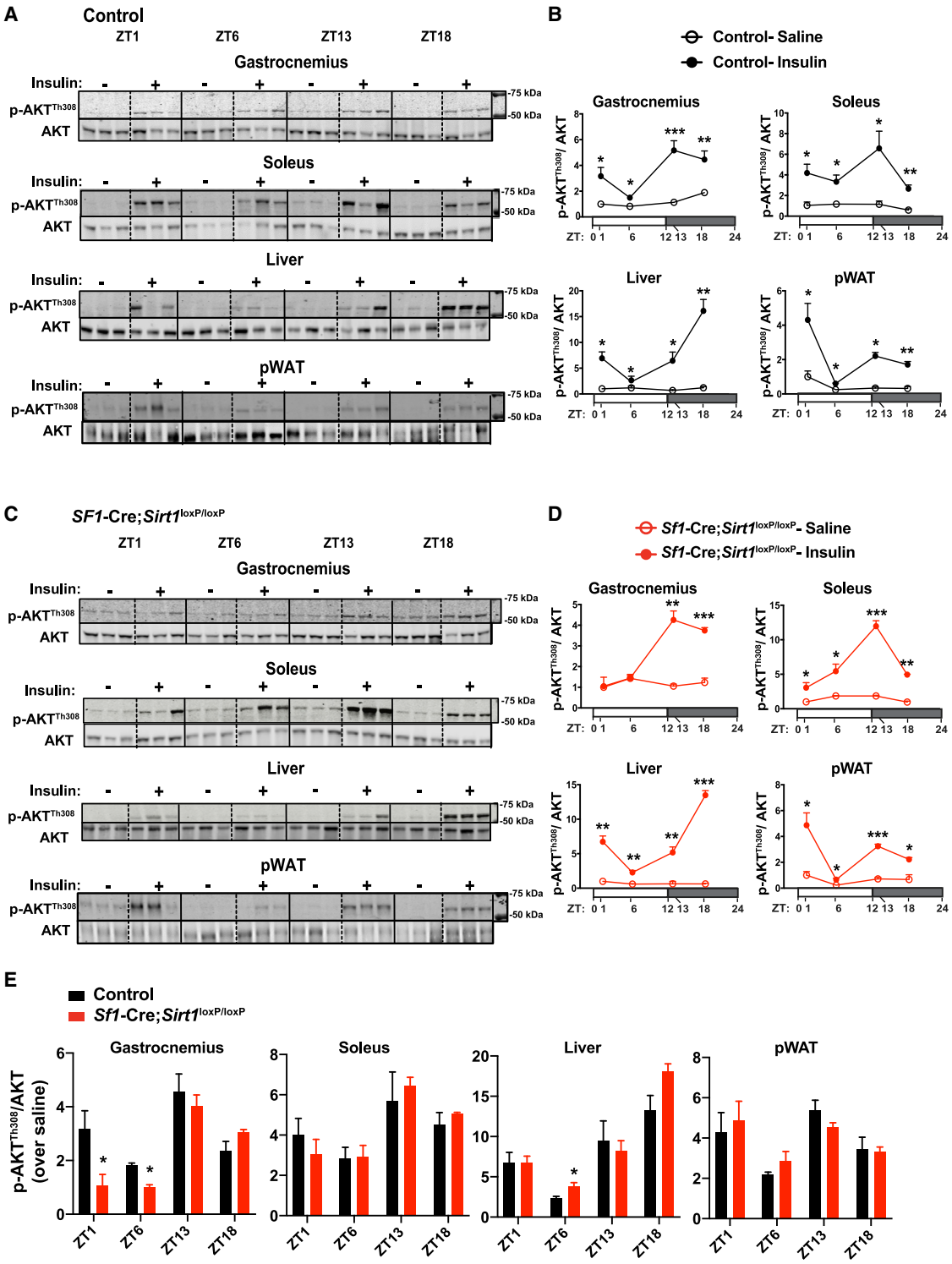

Figure 1. *Sirt1* Deletion in SF1 Neurons Alters Diurnal Magnitude of Insulin Action Selectively in Gastrocnemius

(A and B) Immunoblots from tissues of control mice (A) and relative protein quantifications (B).

(C and D) Immunoblots from tissues of *Sf1*-Cre; *Sirt1*$^{loxP/loxP}$ mice (C) and relative protein quantifications (D).

(E) Relative comparison of insulin-induced p-AKT/AKT between *Sf1*-Cre; *Sirt1*$^{loxP/loxP}$ mice and their controls.

(legend continued on next page)

administration (Coppari and Bjørbæk, 2012; Detournay et al., 2005; Koro et al., 2004). However, in part because of insulin-induced hypoglycemia (a potentially fatal event), insulin therapy is sub-optimal (Coppari and Bjørbæk, 2012; Cryer, 2004, 2006, 2008; Swinnen et al., 2009). In practice, the amount of administered insulin is strictly functional to carbohydrate intake, but the time of day at which insulin is delivered is poorly considered. However, if insulin sensitivity varies around the clock, the time of insulin administration must also be taken into account.

Mammalian diurnal rhythms are driven by internal clocks coordinating the cyclic expression of 10%–20% of genes (Masri and Sassone-Corsi, 2010). Positive (CLOCK/BMAL1 and NPAS2/BMAL1) and negative (PER1/2 and CRY1/2) arms constitute the circadian clock core loop. They generate molecular rhythms that are influenced by nuclear receptors REV-ERBs and RORs, which maintain rhythm stability and strength (Zhang and Kay, 2010). These oscillations can be self-sustained and cell autonomous (Nagoshi et al., 2004). However, in mammals, the peripheral clocks are robustly entrained by light-dark cycles through central mechanisms. These include photic inputs registered by retinal neurons, which are then conveyed to the suprachiasmatic nucleus of the hypothalamus (SCN) via the retinohypothalamic tract (Takahashi, 2017). In a hierarchical manner, SCN cells compute these inputs and relay this information to an ill-characterized downstream neurocircuitry coordinating diurnal oscillations in peripheral tissues (Brancaccio et al., 2019; Takahashi et al., 2008). Neurons within the ventromedial hypothalamic nucleus (VMH) are known to control sympathetic nervous system (SNS) outputs to, and insulin sensitivity in, skeletal muscle in mice (Minokoshi et al., 1999; Ramadori et al., 2011; Shiuchi et al., 2009; Toda et al., 2013). Of note, via polysynaptic pathways, the activity of these VMH neurons is governed by the SCN (Takahashi, 2017; Takahashi et al., 2008; Todd et al., 2018). Also, by targeted ablation of *Bmal1* (a core-clock gene) only in a sub-set of VMH neurons, namely, the steroidogenic factor 1 (SF1) neuron, we have shown that these neurons coordinate diurnal energy expenditure (Orozco-Solis et al., 2016). Hence, although the relevance of these non-SCN brain neurons in maintaining synchronization between external ZTs and endogenous diurnal rhythms is still poorly understood (Asher and Sassone-Corsi, 2015), VMH SF1 neurons appear to exert an important function.

Here, we hypothesized that the insulin sensitivity of key metabolic tissues (e.g., skeletal muscle, adipose tissue, liver) varies across the 24 h daily cycle and that VMH SF1 neurons regulate this rhythm in peripheral insulin action. To test this idea, we first performed a comprehensive assessment of insulin action in metabolically relevant tissues and found ample diurnal oscillation in its magnitude. Next, we generated genetically engineered mice lacking either *Bmal1* or *Sirt1* (whose protein product deacetylates BMAL1 to affect core-clock function; Nakahata et al., 2008) specifically in VMH SF1 neurons. By performing loss- and gain-of-light-action and food-restriction experiments and by assessing the biochemical (e.g., phosphorylation of protein kinase B and glycogen synthase kinase 3 beta) and metabolic (e.g., tissue glucose uptake) consequences of insulin administration, we unraveled a key role of light input in affecting insulin sensitivity in skeletal muscle. Our work reveals that light entrains diurnal changes in clock gene expression and insulin sensitivity in skeletal muscle via SIRT1 in SF1 neurons, an effect that appears to be independent of the VMH-SCN core clock.

RESULTS

To directly test whether tissue insulin sensitivity fluctuates across the daily cycle, mice were kept in a cycle of 12 h light and 12 h dark (LD), and tissue insulin sensitivity was measured at different time points. Phosphorylation of protein kinase B (AKT) and glycogen synthase kinase 3 beta (GSK3β) is a well-established event following the activation of the insulin receptor (Manning and Cantley, 2007; Ramadori et al., 2015). Thus, insulin sensitivity was assessed by quantification of the phosphorylation status of these proteins after an intraperitoneal bolus of the hormone. In gastrocnemius, soleus, and liver, the basal levels of p-GSK3β/GSK3β were not different around the clock (Figures S1A and S1B). In the aforementioned tissues and perigonadal white adipose tissue (pWAT), the basal levels of p-AKT/AKT did not display changes around the clock (Figures 1A and 1B). Insulin administration increased the p-AKT/AKT and p-GSK3β/GSK3β ratios (Figures 1A, 1B, S1A, and S1B). However, the magnitude of insulin-induced phosphorylation of AKT and GSK3β displayed a diurnal pattern, with large differences between times around the clock (Figures 1A, 1B, 1E, S1A, S1B, and S1H). Interestingly, tissue insulin sensitivity was lowest during the resting period (e.g., ZT6) (Figures 1A, 1B, 1E, S1A, S1B, and S1H), which in rodents, in contrast to humans, is throughout the light cycle. Thus, our data demonstrate that in metabolically relevant tissues, the magnitude of insulin action varies around the clock.

The circadian machinery is coupled to metabolism through a mechanism involving the NAD^+-dependent deacetylase SIRT1 that by changing the acetylation status of BMAL1 and PER2 affects their activity and stability, respectively (Asher et al., 2008; Nakahata et al., 2008). Interestingly, although the role of SIRT1 in regulating the circadian clock in a cell-autonomous fashion is established (Asher et al., 2008; Nakahata et al., 2008) whether SIRT1 can affect the circadian clock in a cell-non-autonomous fashion and at distant sites is unknown. We previously showed that mice with altered SIRT1 in VMH SF1 neurons display insulin resistance restrictedly in gastrocnemius skeletal muscle, a defect favoring the development of diabetes (Ramadori et al., 2011). Thus, we hypothesized that SIRT1 in VMH SF1 neurons is part of the underlying molecular mechanism regulating diurnal changes in insulin action in skeletal muscle. To directly test this hypothesis, we generated mice lacking SIRT1 in SF1 neurons by breeding a Cre-conditional *Sirt1*-null allele ($Sirt1^{loxP}$) with a

Data represented in (A)–(E) were obtained from 10-week-old male mice (n = 3 of each genotype). Control mice were homozygous for a $Sirt1^{loxP}$ allele ($Sirt1^{loxP/loxP}$ mice) and were littermates of *Sf1*-Cre; $Sirt1^{loxP/loxP}$ mice. Tissues were collected 20 min after an intraperitoneal bolus of insulin (3 U/kg) or saline. Statistical analyses were done using two-tailed unpaired Student's t test (*$p < 0.05$, **$p < 0.01$, and ***$p < 0.001$).
See also Figure S1.

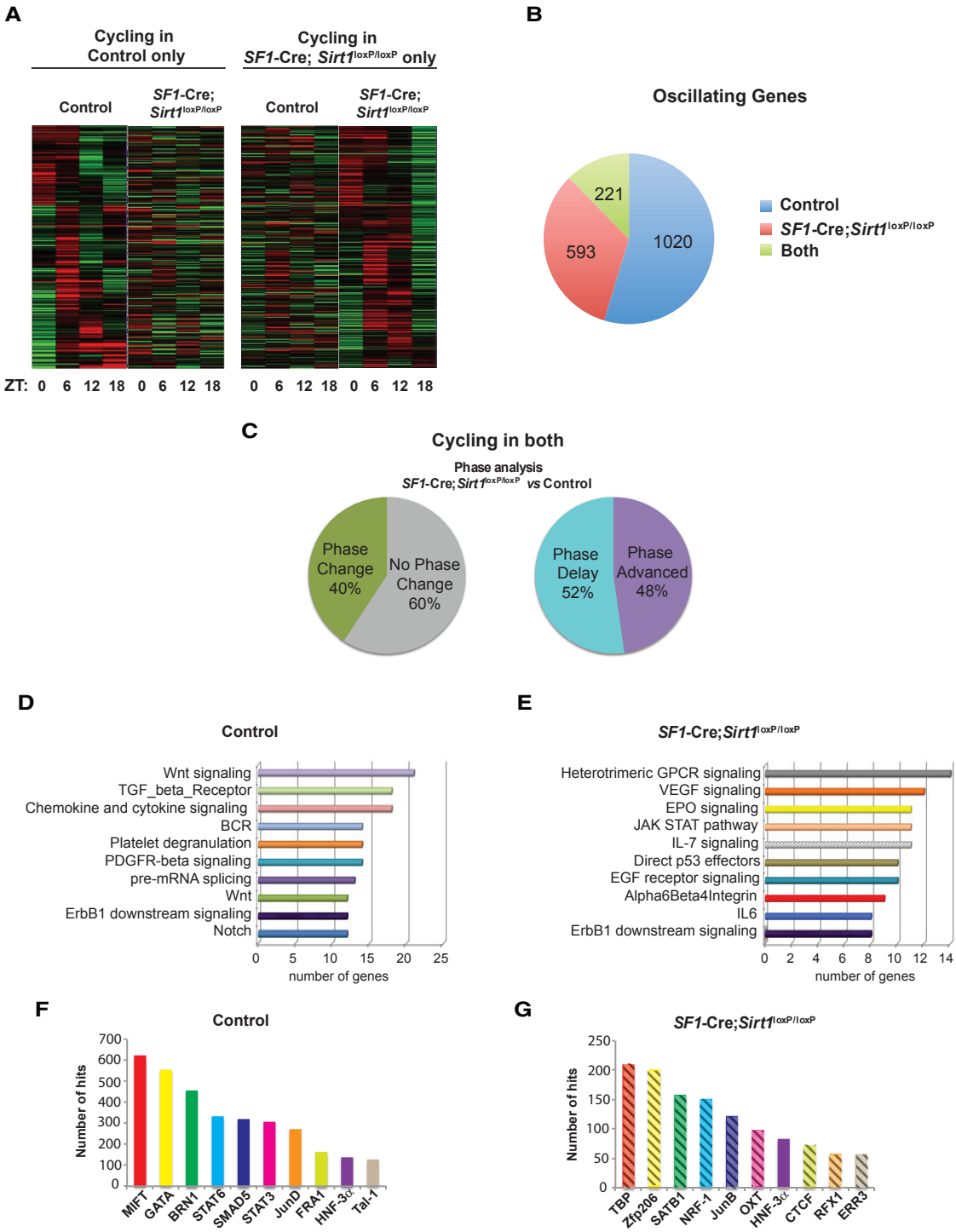

Figure 2. SIRT1 in SF1 Controls the Diurnal Transcriptome in Skeletal Muscle

(A) RNA-seq analysis was performed using total RNA from gastrocnemius of 10-week-old male *Sf1*-Cre; *Sirt1*$^{loxP/loxP}$ mice and controls (*Sirt1*$^{loxP/loxP}$ mice) (n = 4 per group) at ZT 0, 6, 12, and 18. Using the BIO_CYCLE algorithm, genes selected to be diurnal at a p value < 0.05 are displayed as heatmaps for controls and *Sf1*-Cre; *Sirt1*$^{loxP/loxP}$ mice.

(B) Pie chart indicating actual numbers of diurnal genes that oscillate exclusively in controls, *Sf1*-Cre; *Sirt1*$^{loxP/loxP}$ mice, and both groups.

(C) Phase analysis of transcripts oscillating in both controls and in *Sf1*-Cre; *Sirt1*$^{loxP/loxP}$ mice. Left pie chart represents percentage of oscillating transcripts with phase-shift change between *Sf1*-Cre; *Sirt1*$^{loxP/loxP}$ mice and controls of at least 1 h; right pie chart represents percentage of phase delay and phase advance among transcript with phase shift between *Sf1*-Cre; *Sirt1*$^{loxP/loxP}$ mice and controls.

(legend continued on next page)

Sf1-Cre transgene expressing Cre recombinase only in SF1 cells (Ramadori et al., 2011). Genotyping PCR analysis of several tissues of *Sf1*-Cre mice homozygous for the *Sirt1*^{loxP} allele (hereafter referred to as *Sf1*-Cre; *Sirt1*$^{loxP/loxP}$ mice) indicated the presence of the Cre-deleted *Sirt1* allele only in VMH (Figure S1C). In addition, real-time qPCR assay revealed reduced *Sirt1* mRNA content in micro-dissected VMH tissue of *Sf1*-Cre; *Sirt1*$^{loxP/loxP}$ compared with *Sirt1*$^{loxP/loxP}$ control mice (Figure S1D). Furthermore, immunohistochemistry analyses showed that although SIRT1 abundance is unchanged in VMH-neighboring nuclei (e.g., the arcuate nucleus of the hypothalamus [ARH] and dorsomedial nucleus of the hypothalamus [DMH]), it is restrictedly diminished in the VMH of *Sf1*-Cre; *Sirt1*$^{loxP/loxP}$ mice compared with controls (Figure S1E). These results are in line with previous reports demonstrating that *Sf1*-Cre; *Sirt1*$^{loxP/loxP}$ mice lack SIRT1 only in SF1 neurons (Orozco-Solis et al., 2015; Ramadori et al., 2011).

Similar to controls (Figures 1A, 1B, S1A, and S1B), we found that in gastrocnemius, soleus, liver, and pWAT of *Sf1*-Cre; *Sirt1*$^{loxP/loxP}$ mice, basal levels of p-AKT/AKT and p-GSK3β/GSK3β remained constant around the clock (Figures 1C, 1D, and S1F–S1H). Furthermore, in soleus and pWAT of *Sf1*-Cre; *Sirt1*$^{loxP/loxP}$ mice, insulin administration elevated p-AKT/AKT and p-GSK3β /GSK3β, with a pattern of diurnal oscillation and levels similar to controls (Figures 1E and S1H). In liver of *Sf1*-Cre; *Sirt1*$^{loxP/loxP}$ mice, insulin administration increased p-AKT/AKT and p-GSK3β /GSK3β, with a pattern of fluctuation and level quasi-similar to controls, as at ZT6 this effect was slightly enhanced (Figures 1E and S1H). Interestingly, *Sf1*-Cre; *Sirt1*$^{loxP/loxP}$ mice displayed blunted insulin-induced p-AKT/AKT and p-GSK3β/GSK3β in gastrocnemius skeletal muscle, and this defect was selective to the light phase (e.g., ZT1 and ZT6) (Figures 1E and S1H). Of note, this light phase- and gastrocnemius-restricted insulin resistance was independent of differences in body weight or diurnal pattern of glycemia, insulinemia, corticosteronemia, and locomotor activity, as these parameters were similar between genotypes (Figures S1I–S1K) (Orozco-Solis et al., 2015; Ramadori et al., 2011). Together, our data suggest that diurnal changes in insulin sensitivity in gastrocnemius skeletal muscle is remotely controlled by SIRT1 in SF1 neurons.

To gain insight into the mechanism underlying this VMH-gastrocnemius daily axis, mice were sacrificed every 6 h over the 24 h cycle, and gastrocnemius transcriptomic analysis was performed. Global gene expression analysis using the BIO_CYCLE algorithm (Agostinelli et al., 2016) revealed a striking difference in sets of oscillating genes between *Sf1*-Cre; *Sirt1*$^{loxP/loxP}$ mice and their controls (Figure 2A; Table S1). In gastrocnemius of controls, we found 1,241 oscillatory transcripts, of which only 221 were rhythmic also in *Sf1*-Cre; *Sirt1*$^{loxP/loxP}$ mice (Figure 2B; Table S1). However, 40% of these commonly oscillating transcripts exhibited a shift in phase (52% were delayed while 48% were advanced in phase) in *Sf1*-Cre; *Sirt1*$^{loxP/loxP}$ mice (Figure 2C; Table S1). Interestingly, we also found that 593 transcripts acquired *de novo* diurnal rhythmicity, as they were exclusively oscillatory in gastrocnemius of *Sf1*-Cre; *Sirt1*$^{loxP/loxP}$ mice (Figure 2B; Table S1). Gene Ontology (GO) analysis revealed that in controls, the oscillating genes were enriched for a number of metabolic processes and inflammatory signaling (Figure 2D; Table S1). On the other hand, in *Sf1*-Cre; *Sirt1*$^{loxP/loxP}$ mice, the oscillating genes were selectively enriched for a completely different set of pathways (Figure 2E; Table S1). Of note, a number of mRNA changes identified by RNA sequencing (RNA-seq) transcriptomic analysis were independently confirmed by qPCR assay. For example, genes that were found to be specifically oscillating in controls (e.g., *Vegf*, *Hes1*, *Myh2*) or in *Sf1*-Cre; *Sirt1*$^{loxP/loxP}$ mice (e.g., *Pik3*, *Prkca*, *Pten*) were confirmed by qPCR assay (Figures S2A and S2B). Of note, we also found that the acquired diurnal transcriptome rhythmicity in gastrocnemius of *Sf1*-Cre; *Sirt1*$^{loxP/loxP}$ mice was tissue specific. Indeed, genes that were found to oscillate only in gastrocnemius of *Sf1*-Cre; *Sirt1*$^{loxP/loxP}$ mice (Figure 2B) displayed normal expression in soleus, liver, and pWAT of *Sf1*-Cre; *Sirt1*$^{loxP/loxP}$ mice (Figure S3A). Next, we performed a transcription factor motif analysis in order to determine the frequency of specific transcription factor binding sites on the promoters of genes that were specifically oscillating in gastrocnemius of control or *Sf1*-Cre; *Sirt1*$^{loxP/loxP}$ mice (Figures 2F and 2G). These data revealed that only one of the ten most represented transcription factors is shared between genotypes (Figures 2F and 2G). In gastrocnemius of *Sf1*-Cre; *Sirt1*$^{loxP/loxP}$ mice, the diurnal mRNA content of core-clock (*Bmal1*, *Cry2*, *Per2*, and *Rev-erbα*) and clock-controlled (*Pgc-1α* and *Sirt1*) genes as well as the protein content of BMAL1 and PGC-1α were significantly anomalous (Figures 3A–3C, S3B, and S3C). On the other hand, the same transcripts were oscillating normally in soleus, liver, and pWAT of *Sf1*-Cre; *Sirt1*$^{loxP/loxP}$ mice (Figure 3B). Collectively, our data demonstrate that SIRT1 in SF1 neurons remotely coordinates circadian clock function selectively in gastrocnemius skeletal muscle.

To understand how SF1 neurons control circadian clock function in gastrocnemius, we focused on the SNS, as activation of beta-adrenergic receptors (β-ARs) has been shown to regulate metabolic pathways in skeletal muscle (Shiuchi et al., 2009, 2017). Of note, phosphorylation of beta-2-adrenergic receptor (β-2AR) at serine residues 355 and 356 (Ser$^{355/356}$) has been used as a readout of increased SNS action (Fan et al., 2016). Therefore, we examined whether the activation of SNS in gastrocnemius is altered in *Sf1*-Cre; *Sirt1*$^{loxP/loxP}$ mice. Our data shown in Figures 3D and S3D indicate that phosphorylation of β-2AR at Ser$^{355/356}$ is significantly reduced in *Sf1*-Cre; *Sirt1*$^{loxP/loxP}$ mice. These results suggest that SF1 neurons coordinate clock function in gastrocnemius skeletal muscle in part via the SNS.

SIRT1 deacetylates BMAL1, which is a key component of the core-clock mechanism (Nakahata et al., 2008). Hence, one

(D and E) Top ten Gene Ontology (GO) terms for biological processes on the basis of a p value cutoff of 0.01 in (D) controls and (E) *Sf1*-Cre; *Sirt1*$^{loxP/loxP}$ mice. (F and G) Number of oscillating genes containing promoter region recognized by the indicated transcription factors in gastrocnemius of (F) control mice and (G) *Sf1*-Cre; *Sirt1*$^{loxP/loxP}$ mice, analyzed using MotifMap (see STAR Methods): top ten transcription factors on the basis of major number of hits and p value cutoff of 0.01.

See also Figure S2 and Table S1.

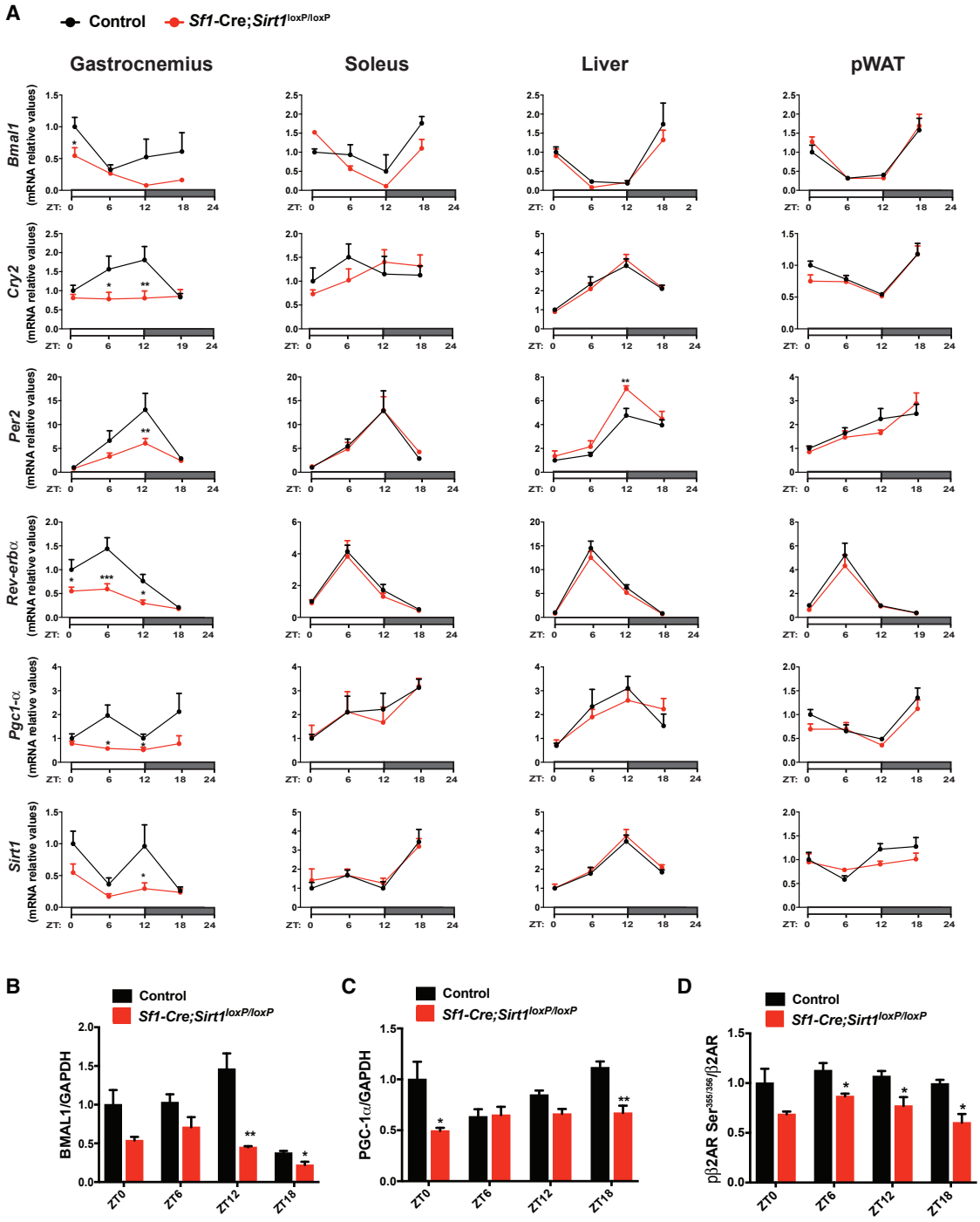

Figure 3. SIRT1 in SF1 Controls the Diurnal Clock Specifically in Skeletal Muscle

(A) Diurnal mRNA levels of *Bmal1*, *Cry2*, *Per2*, *Rev-erbα*, *Pgc1α*, and *Sirt1* in gastrocnemius, soleus, liver, and pWAT of 10-week-old *Sf1*-Cre; *Sirt1*$^{loxP/loxP}$ male mice and their *Sirt1*$^{loxP/loxP}$ controls in LD (n = 6–8 of each group/ZT).

(B–D) Relative protein quantification of (B) BMAL1, (C) PGC1α, and (D) phosphorylated β-2AR Ser$^{355/356}$/β-2AR in gastrocnemius of 10-week-old *Sf1*-Cre; *Sirt1*$^{loxP/loxP}$ male mice and controls in LD (n = 3 of each group).

Error bars represent SEM. Statistical analyses were done using two-tailed unpaired Student's t test (*p < 0.05, **p < 0.01, and ***p < 0.001).

See also Figures S3–S5.

cellular mechanism by which SIRT1 in SF1 neurons could influence diurnal changes in gastrocnemius skeletal muscle function is via regulation of BMAL1 in SF1 neurons. Therefore, if BMAL1 is required for SIRT1 in SF1 neurons to govern diurnal rhythms in gastrocnemius, then lack of BMAL1 in SF1 neurons should lead to altered rhythms in this tissue. To test this hypothesis, we performed experiments in mice lacking BMAL1 in SF1 neurons. SF1 neuron-specific deletion of the core-clock component *Bmal1* was achieved by generating *Sf1*-Cre; *Bmal1*$^{loxP/loxP}$ mice (Orozco-Solis et al., 2016). These mice and their *Bmal1*$^{loxP/loxP}$ controls were maintained with food and water available *ad libitum*, kept on a normal LD cycle, and sacrificed at different ZTs. As previously shown in Figure 3A, diurnal expression of core-clock genes *Bmal1*, *Cry2*, *Per2*, and *Rev-erbα* and clock-controlled genes *Pgc-1α* and *Sirt1* was significantly altered in gastrocnemius of *Sf1*-Cre; *Sirt1*$^{loxP/loxP}$ mice. However, expression of these same genes was normal in gastrocnemius of *Sf1*-Cre; *Bmal1*$^{loxP/loxP}$ mice (Figure S4A). Furthermore, the diurnal oscillation in BMAL1 and PGC-1α protein content found to be slightly blunted in gastrocnemius of *Sf1*-Cre; *Sirt1*$^{loxP/loxP}$ mice (Figures 3B, 3C, S3B, and S3C) was normal in *Sf1*-Cre; *Bmal1*$^{loxP/loxP}$ mice (Figure S4B). These data demonstrate that BMAL1 in SF1 neurons is dispensable for normal diurnal variation in gene expression in gastrocnemius.

One of the major outputs of the core clock in SF1 neurons is regulation of daily thermal oscillation in interscapular brown adipose tissue (iBAT) (Orozco-Solis et al., 2016). Thus, to determine whether SIRT1 deletion in SF1 neurons alters core-clock function in SF1 neurons, we measured iBAT temperature every 6 h over the 24 h cycle. As expected, iBAT temperature displayed diurnal oscillation in control mice, and this rhythmicity was normal in *Sf1*-Cre; *Sirt1*$^{loxP/loxP}$ mice (Figures S5A and S5B). In addition, deletion of SIRT1 in SF1 neurons did not alter the expression of core-clock genes in VMH and SCN, as mRNA levels of *Bmal1*, *Cry2*, *Per2*, and *Rev-erbα* in these micro-dissected nuclei were not different between *Sf1*-Cre; *Sirt1*$^{loxP/loxP}$ mice and their controls (Figures S5C and S5D). Altogether, these data suggest that the core clock in SF1 neurons and in SCN is unaffected by SIRT1 deletion in SF1 neurons and that SIRT1 in SF1 neurons remotely governs diurnal rhythms in gastrocnemius skeletal muscle in a VMH-SCN-core-clock-independent manner.

To determine the signal(s) coordinating gastrocnemius circadian clock, we focused on feeding and photic inputs, as they are major ZTs. In rodents, feeding activity occurs mostly during the dark cycle, and feeding inputs can robustly reshape peripheral clocks independently of light-dark cycles (Asher and Sassone-Corsi, 2015). Thus, we tested the effect of restricted feeding during the 12 h light phase in mice housed in the normal 12 h light and 12 h dark cycle (LD-RFL) (Figure 4A). Of note, 6 days of LD-RFL reshaped diurnal expression and phase distribution of core-clock genes (e.g., *Bmal1*, *Cry2*, *Per2*, and *Rev-erbα*) and clock-controlled genes (e.g., *Pgc-1α* and *Sirt1*) in gastrocnemius of control mice, as these parameters were changed compared with the *ad libitum* feeding condition (Figures 3A and 4B–4D). For example, whereas *Bmal1* and *Cry2* mRNA levels normally peak at ZT21 and ZT9, LD-RFL shifted these peaks to ZT16 and ZT2, respectively (Figure 4C). This is 5–7 h of phase delay compared with the *ad libitum* condition. Of note, LD-RFL reshaped diurnal expression and phase distribution of core-clock and clock-controlled genes in gastrocnemius of *Sf1*-Cre; *Sirt1*$^{loxP/loxP}$ mice compared with the *ad libitum* feeding context and to a level similar to control mice with LD-RFL (Figures 3A and 4B–4D). For example, LD-RFL shifted the peaks of *Bmal1* and *Cry2* mRNA levels from ZT0/ZT1 and ZT18/19 to ZT16 and ZT3, respectively (Figure 4C). These results demonstrate that feeding inputs reshape diurnal expression in gastrocnemius of *Sf1*-Cre; *Sirt1*$^{loxP/loxP}$ mice similarly to controls. Thus, SIRT1 in SF1 neurons is not required for relaying feeding inputs to clock function in gastrocnemius skeletal muscle.

Next, to determine the role of light inputs, we performed loss- and gain-of-function experiments. Housing mice in constant darkness (DD) achieved loss of photic input. As we have shown previously (Orozco-Solis et al., 2016), *Sf1*-Cre; *Sirt1*$^{loxP/loxP}$ mice display normal wheel-running activity in LD and in DD (Figure S6A). Thus, because the activity phase shift induced by DD was similar between *Sf1*-Cre; *Sirt1*$^{loxP/loxP}$ and control mice (Figure S6B), we performed direct comparative analysis between these groups. Thirty days of DD reshaped circadian expression and phase distribution of several core-clock (e.g., *Bmal1*, *Cry2*, *Per2*, and *Rev-erbα*) and clock-controlled (e.g., *Pgc-1α* and *Sirt1*) genes in gastrocnemius of control mice (Figures 3A and 5A–5C). For example, whereas *Cry2* and *Per2* mRNA levels normally peak at ZT9 and ZT11, DD shifted these peaks to circadian time [CT] 12 and CT14/15, respectively (Figure 5B). This is 3–4.5 h of phase delay. Of note, DD reshaped circadian expression and phase distribution of core-clock and clock-controlled genes in gastrocnemius of *Sf1*-Cre; *Sirt1*$^{loxP/loxP}$ mice compared with the *ad libitum* feeding condition and for core-clock genes (*Bmal1*, *Cry2*, *Per2*, and *Rev-erbα*) to a level similar to control mice in DD (Figures 3A and 5A–5C). For example, DD shifted the peaks of *Cry2* and *Per2* mRNA levels from ZT18/ZT19 and ZT11 to CT12 and CT15, respectively (Figure 5B). Because light removal rescued the core-clock defect observed in gastrocnemius, our data suggest that SIRT1 in SF1 neurons relays photic inputs to gastrocnemius circadian clock. To further address this possibility, photic gain-of-function experiments were performed by exposing mice to 1 h light input in the middle of the dark cycle for 30 days (LDL) (Figure 5D). Although LDL did not influence the free-running period, it changed the activity pattern during the light-off period compared with the LD context; yet this activity pattern change was similar between *Sf1*-Cre; *Sirt1*$^{loxP/loxP}$ mice and their controls (Figure S6C). Also, LDL did not have an impact on body weight and food intake, and these parameters were not different between genotypes (Figures S6D and S6E). Interestingly, LDL reshaped the diurnal expression and phase distribution of several core-clock (e.g., *Bmal1*, *Cry2*, *Per2*, and *Rev-erbα*) and clock-controlled (e.g., *Pgc-1α* and *Sirt1*) genes in gastrocnemius of control mice (Figures 3A and 5E–5G). For example, whereas *Bmal1* and *Cry2* mRNA levels normally peak at ZT21 and ZT9, LDL shifted these peaks to ZT16 and ZT6, respectively (Figures 4C and 5E–5G). This is 3–7 h of phase advance. Of note, the ability of light to reshape the circadian clock in gastrocnemius was significantly blunted in *Sf1*-Cre; *Sirt1*$^{loxP/loxP}$ mice (Figures 5E–5G). In fact, phase distribution of core-clock and clock-controlled genes was similar between

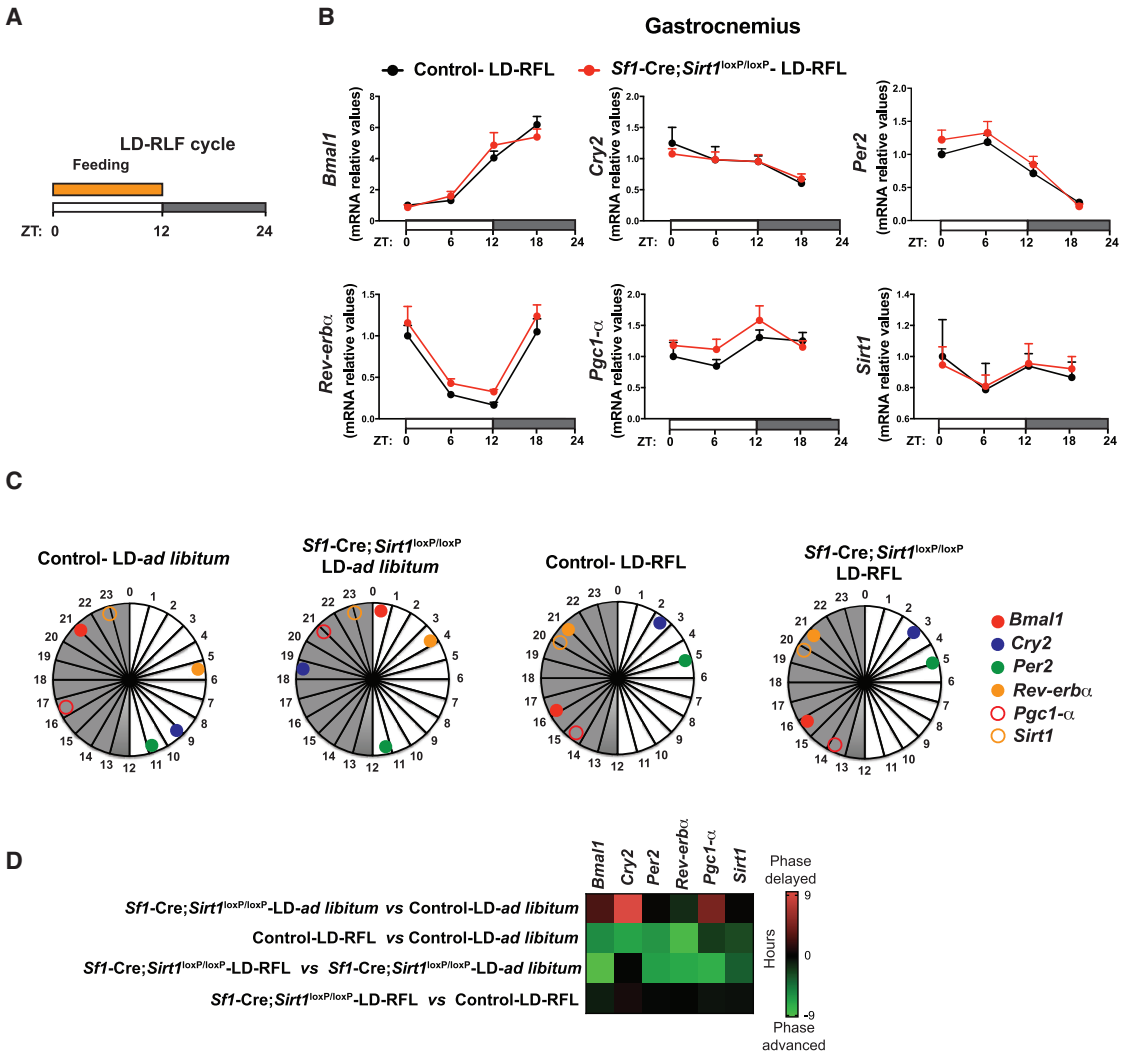

Figure 4. SIRT1 in SF1 Neurons Is Not Required for Feeding Entrainment of Skeletal Muscle Diurnal Clock

(A) Timetable describing LD-RFL cycle: mice were exposed to a 12 h light, 12 h dark cycle with food available only during the 12 h light phase.

(B) Diurnal mRNA levels of *Bmal1*, *Cry2*, *Per2*, *Rev-erbα*, *Pgc1α*, and *Sirt1* in gastrocnemius of 10-week-old *Sf1*-Cre; *Sirt1*$^{loxP/loxP}$ male mice and their *Sirt1*$^{loxP/loxP}$ controls on LD-RFL (n = 7–9 per group).

(C) Diagrams representing phase distribution of mRNA levels of *Bmal1*, *Cry2*, *Per2*, *Rev-erbα*, *Pgc1α*, and *Sirt1* in gastrocnemius of *Sf1*-Cre; *Sirt1*$^{loxP/loxP}$ and their *Sirt1*$^{loxP/loxP}$ controls in LD (fed *ad libitum*) and LD-RLF.

(D) Heatmap representing phase shift (phase delayed and phase advanced) of gastrocnemius mRNA levels of *Bmal1*, *Cry2*, *Per2*, *Rev-erbα*, *Pgc1α*, and *Sirt1* between the represented mouse groups in LD fed either *ad libitum* or RLF.

Error bars represent SEM. Statistical analyses were done using two-tailed unpaired Student's t test and showed no differences.

gastrocnemius of *Sf1*-Cre; *Sirt1*$^{loxP/loxP}$ mice in LD and in LDL, hence demonstrating the inability of *Sf1*-Cre; *Sirt1*$^{loxP/loxP}$ mice to respond to photic input (Figures 5F and 5G). Collectively, our data indicate SIRT1 in SF1 neurons is required for light-induced entrainment of the circadian clock in gastrocnemius skeletal muscle.

To test whether photic inputs are required for normal insulin sensitivity, we exposed mice for 2 days to DD (2DD) and assessed their tissue insulin sensitivity. Surprisingly, light removal caused insulin resistance in gastrocnemius and soleus skeletal muscle, as insulin-induced p-AKT/AKT and p-GSK3β/GSK3β in 2DD mice was reduced compared with their LD controls (Figures 6A–6D). Of note, light removal caused a similar deleterious effect in soleus skeletal muscle of *Sf1*-Cre; *Sirt1*$^{loxP/loxP}$ mice, as insulin-induced p-AKT/AKT and p-GSK3β/GSK3β in soleus of *Sf1*-Cre; *Sirt1*$^{loxP/loxP}$ mice kept for 2 days in DD was reduced compared with *Sf1*-Cre; *Sirt1*$^{loxP/loxP}$ mice housed on a normal LD cycle (Figures 6C and 6D). On the other hand, light removal did not affect insulin sensitivity of gastrocnemius skeletal muscle in mice lacking SIRT1 in SF1 neurons, as insulin-induced p-AKT/AKT and p-GSK3β/GSK3β in *Sf1*-Cre; *Sirt1*$^{loxP/loxP}$ mice kept for 2 days in DD was undistinguishable from *Sf1*-Cre; *Sirt1*$^{loxP/loxP}$ mice housed in normal LD cycle (Figures 6A and 6B). Importantly, the action of light removal on insulin action in

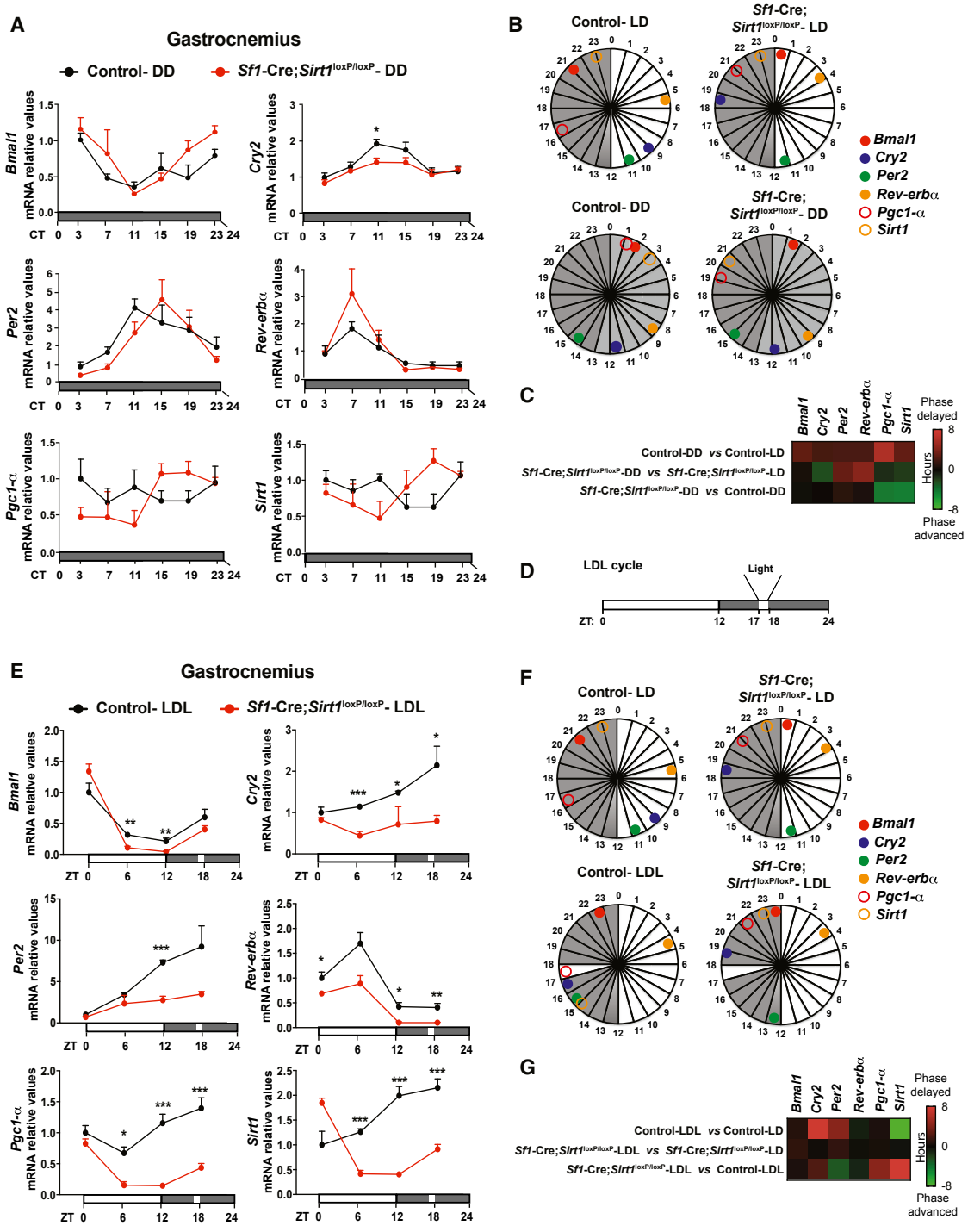

Figure 5. Light Inputs Entrain Circadian Clock in Gastrocnemius via SIRT1 in SF1 Neurons

(A) Circadian mRNA levels of *Bmal1*, *Cry2*, *Per2*, *Rev-erbα*, *Pgc1α*, and *Sirt1* in gastrocnemius of 10-week-old *Sf1*-Cre; *Sirt1*$^{loxP/loxP}$ male mice and their *Sirt1*$^{loxP/loxP}$ controls in DD (n = 5 or 6 per group).

(B) Diagrams representing phase distribution of mRNA levels of *Bmal1*, *Cry2*, *Per2*, *Rev-erbα*, *Pgc1α*, and *Sirt1* in gastrocnemius of *Sf1*-Cre; *Sirt1*$^{loxP/loxP}$ and their *Sirt1*$^{loxP/loxP}$ controls in LD and DD.

(C) Heatmap representing phase shift (phase delayed and phase advanced) of gastrocnemius mRNA levels of *Bmal1*, *Cry2*, *Per2*, *Rev-erbα*, *Pgc1α*, and *Sirt1* between the represented mouse groups.

(D) Timetable describing LDL cycle.

(legend continued on next page)

gastrocnemius skeletal muscle was similar to the effect of SIRT1 deletion in SF1 neurons. In fact, insulin-induced p-AKT/AKT and p-GSK3β/GSK3β in gastrocnemius of 2DD control mice was similar to that found in *Sf1*-Cre; *Sirt1*$^{loxP/loxP}$ mice kept on a normal LD cycle (Figures 6A and 6B).

To further assess the effect of photic loss or gain of function on tissue responsiveness to insulin, measurement of insulin-induced glucose uptake *in vivo* was performed. Interestingly, light removal (2DD) or 1-hour light input in the middle of the dark cycle (LDL) negatively affected insulin-induced glucose uptake in gastrocnemius skeletal muscle of control mice. Indeed, the ability of insulin to stimulate glucose uptake in this tissue of 2DD or LDL mice was reduced compared with LD controls (Figure 6E). Of note, the defect in insulin-induced glucose uptake caused by either 2DD or LDL was similar to that caused by SIRT1 deletion in SF1 neurons. Indeed, there was no difference in insulin-induced glucose uptake in gastrocnemius skeletal muscle of control mice housed in 2DD or LDL conditions and *Sf1*-Cre; *Sirt1*$^{loxP/loxP}$ mice housed in LD cycle (Figure 6E). Importantly, neither 2DD nor LDL affected insulin-induced glucose uptake in gastrocnemius of *Sf1*-Cre; *Sirt1*$^{loxP/loxP}$ mice, hence indicating that SIRT1 in SF1 neurons is required for light-induced entrainment of insulin sensitivity in skeletal muscle (Figure 6E). Collectively, these data demonstrate that altering photic inputs dampens skeletal muscle responsiveness to insulin and that SIRT1 in SF1 neurons is required for light-induced changes in insulin sensitivity in gastrocnemius skeletal muscle.

DISCUSSION

Virtually all physiological functions (e.g., nutrient processing, cardiovascular output, renal filtration, heat production) must be coordinated with light-dark cycles and tied to geophysical time (Bass, 2012; Bass and Takahashi, 2010). These functions are in part orchestrated by diurnal oscillation in hormonal action, and it is common wisdom that daily variation in hormonal secretion is the main driver for achieving changes in hormonal effect. Here we show that diurnal variation in hormonal sensitivity is also crucial for ensuring that the appropriate hormonal action is achieved at the right time. For example, we show that skeletal muscle, adipose tissue, and liver are very sensitive to insulin at times when mice are active and eat (i.e., the dark period), whereas these tissues are more resistant to the hormone when mice are inactive (i.e., the light period). We suggest that these data unveil a physiological mechanism by which the combination of insulin abundance and appropriate tissue responsiveness guarantees that the correct insulin effect is attained at the right time. Specifically, the highest insulin sensitivity during the feeding period would guarantee that insulin-induced glucose uptake is properly achieved during a phase of food intake. On the other hand, the lowest insulin sensitivity during the resting period would guarantee that insulin-induced suppression of endogenous glucose production and free fatty acid secretion are dampened during a fasting phase, when glucose and free fatty acid secretion are needed (Rodgers et al., 2005). Our rodent data are in line with clinical observations indicating that insulin sensitivity is highest at the onset of the feeding period (Carroll and Nestel, 1973; Gibson and Jarrett, 1972; Service et al., 1983; Van Cauter et al., 1991; Whichelow et al., 1974). We propose that diurnal variation in tissue responsiveness to hormonal action is not restricted to insulin and is therefore a broader phenomenon. Hence, further studies aimed at determining whether the sensitivity of other hormones (whose content varies during the 24 h period, e.g., thyroid hormone, glucocorticoids) fluctuates around the clock are warranted.

Here, we show that light inputs affect insulin sensitivity. For example, altering the daily variation in photic inputs either by light gain or loss of action leads to similar defects in insulin sensitivity in skeletal muscle (Figures 6A–6E). These data are in keeping with previous results indicating that exposure to light at the wrong time negatively affects glucose homeostasis (Cheung et al., 2016; Opperhuizen et al., 2017; Versteeg et al., 2017). Mechanistically, we found that light governs insulin sensitivity in gastrocnemius skeletal muscle through a pathway involving SIRT1 in SF1 neurons. Of note, our results bring about new questions. For example, how do photic inputs reach VMH SF1 neurons? First, photic inputs are registered by retinal neurons, then conveyed to SCN neurons, which then relay this information to a poorly characterized neurocircuitry (Takahashi et al., 2008). We suggest that VMH SF1 neurons are part of this circuitry. Indeed, SCN neurons could control VMH SF1 neurons via indirect polysynaptic connections involving paraventricular and dorsomedial hypothalamic nuclei and/or orexin neurons in the lateral hypothalamic area (Ramadori et al., 2011; Saper et al., 2005). Alternatively, because retinal cells project to other non-SCN brain sites, it is possible that these cells project to VMH neurons without the involvement of the SCN. In addition, how do VMH SF1 neurons "communicate" specifically to gastrocnemius skeletal muscle? We suggest at least two possibilities: via neuroendocrine circulating factor(s) and/or the autonomic nervous system. The latter is more likely because it is supported by results from recent studies showing that (1) VMH-centered orexin-A delivery enhances insulin sensitivity in skeletal muscle through increased sympathetic tone in this tissue (Shiuchi et al., 2009), and (2) orexin-A's anti-diabetic action is severely impaired in mice lacking SIRT1 in SF1 neurons (Ramadori

(E) Circadian mRNA levels of *Bmal1*, *Cry2*, *Per2*, *Rev-erbα*, *Pgc1α*, and *Sirt1* in gastrocnemius of 10-week-old *Sf1*-Cre; *Sirt1*$^{loxP/loxP}$ male mice and their *Sirt1*$^{loxP/loxP}$ controls in LDL (n = 3–5 per group).

(F) Diagrams representing phase distribution of mRNA level of *Bmal1*, *Cry2*, *Per2*, *Rev-erbα*, *Pgc1α*, and *Sirt1* in gastrocnemius of *Sf1*-Cre; *Sirt1*$^{loxP/loxP}$ and their *Sirt1*$^{loxP/loxP}$ controls in LD and LDL.

(G) Heatmap representing phase shift (phase delayed and phase advanced) of gastrocnemius mRNA levels of *Bmal1*, *Cry2*, *Per2*, *Rev-erbα*, *Pgc1α*, and *Sirt1* between the represented mouse groups.

In (B) and (F), diagrams relative to phase distribution in LD are replicas from Figure 4C added to this figure for clarity. Error bars represent SEM. Statistical analyses were done using two-tailed unpaired Student's t test (*$p < 0.05$, **$p < 0.01$, and ***$p < 0.001$).

See also Figure S6.

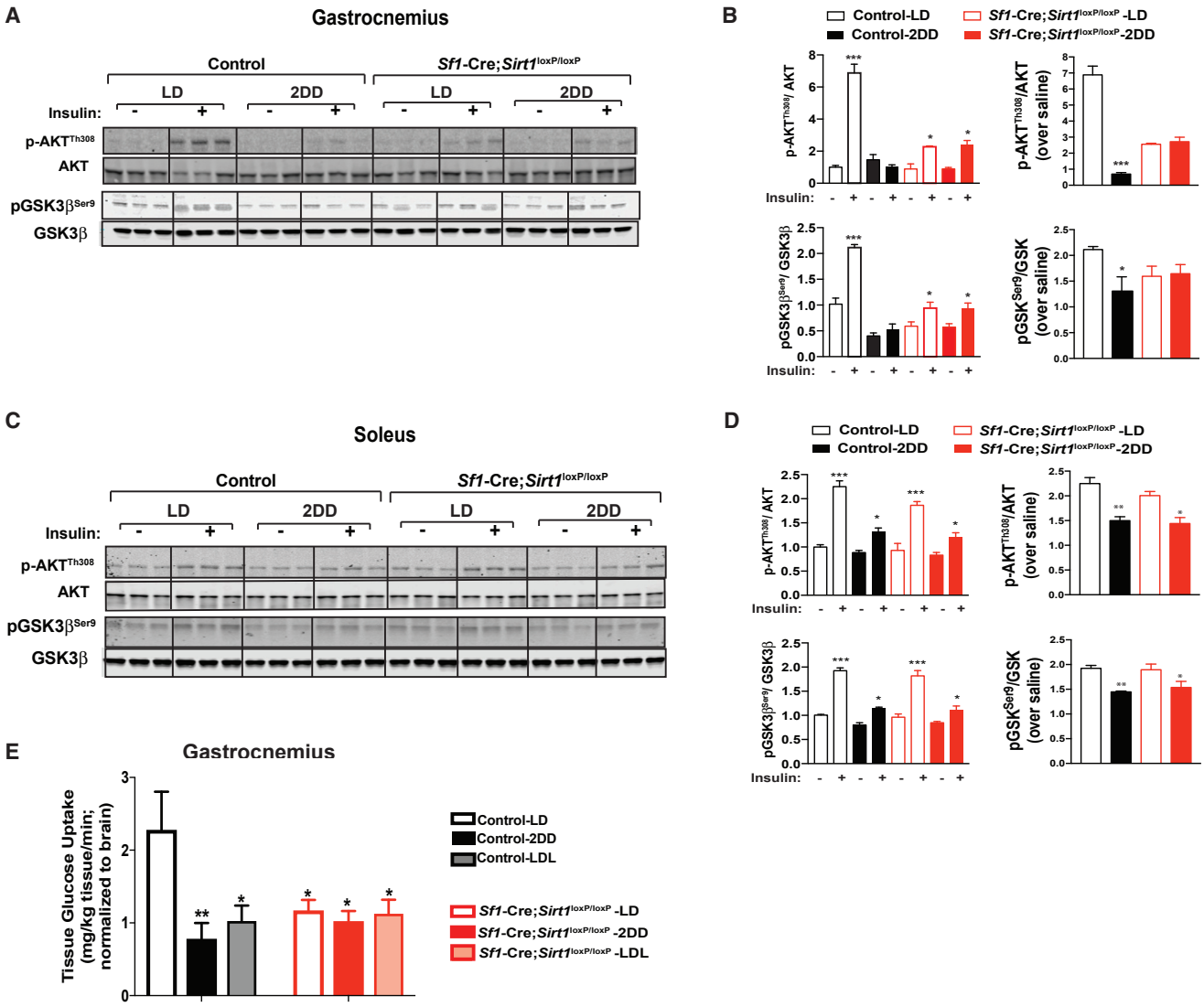

Figure 6. Light Input Controls Skeletal Muscle Insulin Sensitivity through SIRT1 in SF1 Neurons

(A–D) Immunoblots from gastrocnemius (A) and soleus (C) of control mice (*Sirt1*$^{loxP/loxP}$ mice) and *Sf1*-Cre; *Sirt1*$^{loxP/loxP}$ mice. (B and D) Left panel: relative protein quantifications showing p-AKT/AKT and p-GSK3β^{Ser9}/GSK3β. Right panel: relative values of fold increase of insulin-induced p-AKT/AKT and p-GSK3β^{Ser9}/GSK3β over saline level. Immunoblots in (A) and (C) were obtained at ZT6 from 10-week-old male mice (n = 3 of each genotype). Tissues were collected 20 min after an intraperitoneal bolus of insulin (3 U/kg) or saline.

(E) Tissue-specific insulin-stimulated glucose uptake.

Error bars represent SEM. Statistical analyses were done using two-tailed unpaired Student's t test or two-way ANOVA (Tukey's post test). In (B) and (D), left panels: *p < 0.05 and ***p < 0.001, insulin versus saline of same genotype. In (B) and (D), right panels: *p < 0.05, **p < 0.01, and ***p < 0.001, 2DD versus LD of same genotype. In (E), *p < 0.05 and **p < 0.01, all other groups versus control LD.

et al., 2011). Interestingly, in mice, orexin release in the hypothalamus follows a diurnal rhythm, with higher and lower levels during dark and light phases, respectively, similar to the daily variation of insulin signaling in gastrocnemius (Fenzl et al., 2009). Further supporting a role of the SNS, we found reduced phosphorylation status of β2-AR receptor in gastrocnemius of *Sf1*-Cre; *Sirt1*$^{loxP/loxP}$ mice (Figures 3D and S3D). Future studies are necessary to establish the underpinnings of this light-VMH-gastrocnemius circuitry. Importantly, we found that other tissues (i.e., soleus skeletal muscle, liver, and pWAT) display diurnal variation in insulin sensitivity and that this regulation is not controlled by SIRT1 in SF1 neurons. Thus, additional work will be necessary to understand the mechanisms underlying diurnal variation in insulin sensitivity in these other tissues.

A further noteworthy aspect of our results is the concomitant defect in diurnal insulin sensitivity and transcriptome oscillation in gastrocnemius of *Sf1*-Cre; *Sirt1*$^{loxP/loxP}$ mice. We suggest that these two defects are linked to each other, as an altered circadian clock has been shown to impair insulin sensitivity in skeletal muscle. For example, cyclic expression of the essential

core clock component *Bmal1* is severely blunted in gastrocnemius of *Sf1*-Cre; *Sirt1*$^{loxP/loxP}$ mice (Figures 3A and S3B). A previous study indicated that deletion of *Bmal1* in skeletal muscle is sufficient to cause insulin resistance in this tissue (Dyar et al., 2013). Thus, these data would support a causative link between changes in intrinsic circadian clock and reduced insulin sensitivity.

The importance of proper synchronization between light-dark cycles and hormonal action is demonstrated by the fact that when this synchrony is disturbed, metabolic unbalance arises (Masri and Sassone-Corsi, 2013). For example, altered sleep and/or feeding cycles are associated with development of metabolic diseases in humans (Buxton et al., 2012; Scheer et al., 2009). Moreover, genetically engineered animal models bearing an altered circadian clock in either a whole-body or a tissue-specific manner display insulin resistance (Marcheva et al., 2010; McDearmon et al., 2006; Paschos et al., 2012; Shi et al., 2013). Our data could explain, at least in part, why people exposed to light at the wrong times (e.g., shift workers) are more prone to develop diabetes (Masri and Sassone-Corsi, 2013). In fact, we show that light, or the absence of it, can profoundly influence tissue insulin sensitivity and that alteration in this mechanism, as in *Sf1*-Cre; *Sirt1*$^{loxP/loxP}$ mice, is sufficient to favor development of diabetes (Ramadori et al., 2011).

Our results are of important physiological relevance. Indeed, we have previously shown that mice lacking SIRT1 in VMH SF1 neurons are more prone to develop metabolic imbalance (Ramadori et al., 2011). Thus, our data might have clinical relevance. For example, in type 1 diabetes mellitus (T1DM), β-cells are totally (or almost totally) lost (Wasserfall et al., 2017), while in type 2 diabetes mellitus (T2DM), chronic metabolic pressure causes β-cell exhaustion, failure, and/or dedifferentiation (Butler et al., 2007; Talchai et al., 2012). These defects trigger insulin deficiency, an otherwise fatal condition that can be treated only with insulin therapy. However, insulin therapy is unsatisfactory because insulin-deficient patients are still at a much higher risk for developing hypoglycemia (and many other comorbidities) (Larsen et al., 2002; Orchard et al., 2003; Umpierrez and Korytkowski, 2016). Although the amount of injected insulin is based strictly on carbohydrate intake, the time of day when insulin is delivered is poorly considered. Our data indicate that insulin sensitivity varies around the clock. Currently insulin therapy is prescribed to an estimated 100 million people; these include virtually all T1DM patients and ~20%–25% of T2DM patients (Detournay et al., 2005; Koro et al., 2004). Hence, we suggest that the time when insulin is delivered to these patients must be taken into meticulous consideration. In fact, our results suggest that proper calculation, including carbohydrate intake and time of day when insulin is administered, should reduce the risk for insulin-induced hypoglycemia and overall improve diabetes care.

STAR★METHODS

Detailed methods are provided in the online version of this paper and include the following:

- KEY RESOURCES TABLE
- CONTACT FOR REAGENT AND RESOURCE SHARING
- EXPERIMENTAL MODEL AND SUBJECT DETAILS
- METHODS DETAILS
  - Animal Experiments
  - Circadian Behavior
  - Real-Time Quantitative Polymerase Chain Reaction (Real-Time qPCR)
  - Western Blot
  - Blood Chemistry
  - Immunohistochemistry Analyses
  - RNA sequencing and analysis
- QUANTIFICATION AND STATISTICAL ANALYSIS
  - Quantification
  - Statistical Analysis
- DATA AND SOFTWARE AVAILABILITY

SUPPLEMENTAL INFORMATION

Supplemental Information can be found online at https://doi.org/10.1016/j.celrep.2019.04.093.

ACKNOWLEDGMENTS

We thank Ariane Widmer, Anne Charollais, and Carolyn Heckenmeyer in the Coppari laboratory for their technical support and Drs. Ueli Schibler, Claes Wollheim, and Charna Dibner for suggestions and critical reading of the manuscript. We also thank Siwei Chen for helping with gathering the GEO number. This work was supported in part by Coordenação de Aperfeiçoamento de Pessoal de Nível Superior (CAPES graduate student fellowship to R.M.I.), the Bo & Kerstin Hjelt Foundation, the Gertrude von Meissner Foundation (research grant to G.R. and S.L.), the Japan Society for Promotion of Science (JSPS) (postdoctoral fellowship to K.K.), the European Commission (Marie Curie Career Integration Grant 320898 and ERC-Consolidator Grant 614847), the Swiss Cancer League (KLS-3794-02-2016-R), the Louis-Jeantet Foundation, the Gertrude von Meissner Foundation, Fondation Pour Recherches Medicales of the University of Geneva to R.C., and the Swiss National Science Foundation (310030_169966/1 to R.C.).

AUTHOR CONTRIBUTIONS

Conceptualization, R.C., E.A., and G.R.; Investigation, E.A., G.R., K.K., Y.L., R.M.I., X.B., S.L., C.V.-D., S.M., and M.G.; Writing, R.C., E.A., and G.R.; Funding Acquisition, R.M.I., G.R., P.S.-C., P.B., and R.C.; Data Curation, R.C., E.A., P.B., P.S.-C. and G.R.; Supervision, R.C. and G.R.

DECLARATION OF INTERESTS

The authors declare no competing interests.

Received: March 9, 2018
Revised: January 28, 2019
Accepted: April 19, 2019
Published: May 21, 2019

REFERENCES

Agostinelli, F., Ceglia, N., Shahbaba, B., Sassone-Corsi, P., and Baldi, P. (2016). What time is it? Deep learning approaches for circadian rhythms. Bioinformatics *32*, i8–i17.

Anderson, J.G., Ramadori, G., Ioris, R.M., Galiè, M., Berglund, E.D., Coate, K.C., Fujikawa, T., Pucciarelli, S., Moreschini, B., Amici, A., et al. (2015). Enhanced insulin sensitivity in skeletal muscle and liver by physiological overexpression of SIRT6. Mol. Metab. *4*, 846–856.

Asher, G., and Sassone-Corsi, P. (2015). Time for food: the intimate interplay between nutrition, metabolism, and the circadian clock. Cell *161*, 84–92.

Asher, G., Gatfield, D., Stratmann, M., Reinke, H., Dibner, C., Kreppel, F., Mostoslavsky, R., Alt, F.W., and Schibler, U. (2008). SIRT1 regulates circadian clock gene expression through PER2 deacetylation. Cell *134*, 317–328.

Bass, J. (2012). Circadian topology of metabolism. Nature *491*, 348–356.

Bass, J., and Takahashi, J.S. (2010). Circadian integration of metabolism and energetics. Science *330*, 1349–1354.

Brancaccio, M., Edwards, M.D., Patton, A.P., Smyllie, N.J., Chesham, J.E., Maywood, E.S., and Hastings, M.H. (2019). Cell-autonomous clock of astrocytes drives circadian behavior in mammals. Science *363*, 187–192.

Brenachot, X., Ramadori, G., Ioris, R.M., Veyrat-Durebex, C., Altirriba, J., Aras, E., Ljubicic, S., Kohno, D., Fabbiano, S., Clement, S., et al. (2017). Hepatic protein tyrosine phosphatase receptor gamma links obesity-induced inflammation to insulin resistance. Nat. Commun. *8*, 1820.

Butler, P.C., Meier, J.J., Butler, A.E., and Bhushan, A. (2007). The replication of beta cells in normal physiology, in disease and for therapy. Nat. Clin. Pract. Endocrinol. Metab. *3*, 758–768.

Buxton, O.M., Cain, S.W., O'Connor, S.P., Porter, J.H., Duffy, J.F., Wang, W., Czeisler, C.A., and Shea, S.A. (2012). Adverse metabolic consequences in humans of prolonged sleep restriction combined with circadian disruption. Sci. Transl. Med. *4*, 129ra43.

Carrasco-Benso, M.P., Rivero-Gutierrez, B., Lopez-Minguez, J., Anzola, A., Diez-Noguera, A., Madrid, J.A., Lujan, J.A., Martínez-Augustin, O., Scheer, F.A., and Garaulet, M. (2016). Human adipose tissue expresses intrinsic circadian rhythm in insulin sensitivity. FASEB J. *30*, 3117–3123.

Carroll, K.F., and Nestel, P.J. (1973). Diurnal variation in glucose tolerance and in insulin secretion in man. Diabetes *22*, 333–348.

Cerami, E.G., Gross, B.E., Demir, E., Rodchenkov, I., Babur, O., Anwar, N., Schultz, N., Bader, G.D., and Sander, C. (2011). Pathway Commons, a Web resource for biological pathway data. Nucleic Acids Res. *39*, D685–D690.

Cheung, I.N., Zee, P.C., Shalman, D., Malkani, R.G., Kang, J., and Reid, K.J. (2016). Morning and evening blue-enriched light exposure alters metabolic function in normal weight adults. PLoS ONE *11*, e0155601.

Coppari, R., and Bjørbæk, C. (2012). Leptin revisited: its mechanism of action and potential for treating diabetes. Nat. Rev. Drug Discov. *11*, 692–708.

Coppari, R., Ramadori, G., and Elmquist, J.K. (2009). The role of transcriptional regulators in central control of appetite and body weight. Nat. Clin. Pract. Endocrinol. Metab. *5*, 160–166.

Cryer, P.E. (2004). Diverse causes of hypoglycemia-associated autonomic failure in diabetes. N. Engl. J. Med. *350*, 2272–2279.

Cryer, P.E. (2006). Mechanisms of sympathoadrenal failure and hypoglycemia in diabetes. J. Clin. Invest. *116*, 1470–1473.

Cryer, P.E. (2008). The barrier of hypoglycemia in diabetes. Diabetes *57*, 3169–3176.

Czech, M.P. (2017). Insulin action and resistance in obesity and type 2 diabetes. Nat. Med. *23*, 804–814.

Detournay, B., Raccah, D., Cadilhac, M., and Eschwège, E. (2005). Epidemiology and costs of diabetes treated with insulin in France. Diabetes Metab. *31*, 3–18.

Dyar, K.A., Ciciliot, S., Wright, L.E., Biensø, R.S., Tagliazucchi, G.M., Patel, V.R., Forcato, M., Paz, M.I., Gudiksen, A., Solagna, F., et al. (2013). Muscle insulin sensitivity and glucose metabolism are controlled by the intrinsic muscle clock. Mol. Metab. *3*, 29–41.

Eckel-Mahan, K.L., Patel, V.R., Mohney, R.P., Vignola, K.S., Baldi, P., and Sassone-Corsi, P. (2012). Coordination of the transcriptome and metabolome by the circadian clock. Proc. Natl. Acad. Sci. U S A *109*, 5541–5546.

Fan, X., Gu, X., Zhao, R., Zheng, Q., Li, L., Yang, W., Ding, L., Xue, F., Fan, J., Gong, Y., and Wang, Y. (2016). Cardiac β2-adrenergic receptor phosphorylation at Ser355/356 regulates receptor internalization and functional resensitization. PLoS ONE *11*, e0161373.

Fenzl, T., Flachskamm, C., Rossbauer, M., Deussing, J.M., and Kimura, M. (2009). Circadian rhythms of basal orexin levels in the hypothalamus are not influenced by an impaired corticotropin-releasing hormone receptor type 1 system. Behav. Brain Res. *203*, 143–145.

Gamble, K.L., Berry, R., Frank, S.J., and Young, M.E. (2014). Circadian clock control of endocrine factors. Nat. Rev. Endocrinol. *10*, 466–475.

Garaulet, M., Gómez-Abellán, P., Rubio-Sastre, P., Madrid, J.A., Saxena, R., and Scheer, F.A. (2015). Common type 2 diabetes risk variant in MTNR1B worsens the deleterious effect of melatonin on glucose tolerance in humans. Metabolism *64*, 1650–1657.

Gibson, T., and Jarrett, R.J. (1972). Diurnal variation in insulin sensitivity. Lancet *2*, 947–948.

Hughes, M.E., Hogenesch, J.B., and Kornacker, K. (2010). JTK_CYCLE: an efficient nonparametric algorithm for detecting rhythmic components in genome-scale data sets. J. Biol. Rhythms *25*, 372–380.

Ishida, A., Mutoh, T., Ueyama, T., Bando, H., Masubuchi, S., Nakahara, D., Tsujimoto, G., and Okamura, H. (2005). Light activates the adrenal gland: timing of gene expression and glucocorticoid release. Cell Metab. *2*, 297–307.

Kayala, M.A., and Baldi, P. (2012). Cyber-T web server: differential analysis of high-throughput data. Nucleic Acids Res. *40*, W553–W559.

Koro, C.E., Bowlin, S.J., Bourgeois, N., and Fedder, D.O. (2004). Glycemic control from 1988 to 2000 among U.S. adults diagnosed with type 2 diabetes: a preliminary report. Diabetes Care *27*, 17–20.

Larsen, J., Brekke, M., Sandvik, L., Arnesen, H., Hanssen, K.F., and Dahl-Jorgensen, K. (2002). Silent coronary atheromatosis in type 1 diabetic patients and its relation to long-term glycemic control. Diabetes *51*, 2637–2641.

Liu, Y., Sun, S., Bredy, T., Wood, M., Spitale, R.C., and Baldi, P. (2017). MotifMap-RNA: a genome-wide map of RBP binding sites. Bioinformatics *33*, 2029–2031.

Manning, B.D., and Cantley, L.C. (2007). AKT/PKB signaling: navigating downstream. Cell *129*, 1261–1274.

Marcheva, B., Ramsey, K.M., Buhr, E.D., Kobayashi, Y., Su, H., Ko, C.H., Ivanova, G., Omura, C., Mo, S., Vitaterna, M.H., et al. (2010). Disruption of the clock components CLOCK and BMAL1 leads to hypoinsulinaemia and diabetes. Nature *466*, 627–631.

Masri, S., and Sassone-Corsi, P. (2010). Plasticity and specificity of the circadian epigenome. Nat. Neurosci. *13*, 1324–1329.

Masri, S., and Sassone-Corsi, P. (2013). The circadian clock: a framework linking metabolism, epigenetics and neuronal function. Nat. Rev. Neurosci. *14*, 69–75.

McDearmon, E.L., Patel, K.N., Ko, C.H., Walisser, J.A., Schook, A.C., Chong, J.L., Wilsbacher, L.D., Song, E.J., Hong, H.K., Bradfield, C.A., and Takahashi, J.S. (2006). Dissecting the functions of the mammalian clock protein BMAL1 by tissue-specific rescue in mice. Science *314*, 1304–1308.

Minokoshi, Y., Haque, M.S., and Shimazu, T. (1999). Microinjection of leptin into the ventromedial hypothalamus increases glucose uptake in peripheral tissues in rats. Diabetes *48*, 287–291.

Nagoshi, E., Saini, C., Bauer, C., Laroche, T., Naef, F., and Schibler, U. (2004). Circadian gene expression in individual fibroblasts: cell-autonomous and self-sustained oscillators pass time to daughter cells. Cell *119*, 693–705.

Nakahata, Y., Kaluzova, M., Grimaldi, B., Sahar, S., Hirayama, J., Chen, D., Guarente, L.P., and Sassone-Corsi, P. (2008). The NAD+-dependent deacetylase SIRT1 modulates CLOCK-mediated chromatin remodeling and circadian control. Cell *134*, 329–340.

Opperhuizen, A.L., Stenvers, D.J., Jansen, R.D., Foppen, E., Fliers, E., and Kalsbeek, A. (2017). Light at night acutely impairs glucose tolerance in a time-, intensity- and wavelength-dependent manner in rats. Diabetologia *60*, 1333–1343.

Orchard, T.J., Olson, J.C., Erbey, J.R., Williams, K., Forrest, K.Y., Smithline Kinder, L., Ellis, D., and Becker, D.J. (2003). Insulin resistance-related factors, but not glycemia, predict coronary artery disease in type 1 diabetes: 10-year follow-up data from the Pittsburgh Epidemiology of Diabetes Complications Study. Diabetes Care *26*, 1374–1379.

Orozco-Solis, R., Ramadori, G., Coppari, R., and Sassone-Corsi, P. (2015). SIRT1 relays nutritional inputs to the circadian clock through the Sf1 neurons of the ventromedial hypothalamus. Endocrinology *156*, 2174–2184.

Orozco-Solis, R., Aguilar-Arnal, L., Murakami, M., Peruquetti, R., Ramadori, G., Coppari, R., and Sassone-Corsi, P. (2016). The circadian clock in the ventromedial hypothalamus controls cyclic energy expenditure. Cell Metab. *23*, 467–478.

Paschos, G.K., Ibrahim, S., Song, W.L., Kunieda, T., Grant, G., Reyes, T.M., Bradfield, C.A., Vaughan, C.H., Eiden, M., Masoodi, M., et al. (2012). Obesity in mice with adipocyte-specific deletion of clock component Arntl. Nat. Med. *18*, 1768–1777.

Patel, V.R., Eckel-Mahan, K., Sassone-Corsi, P., and Baldi, P. (2012). CircadiOmics: integrating circadian genomics, transcriptomics, proteomics and metabolomics. Nat. Methods *9*, 772–773.

Ramadori, G., Fujikawa, T., Fukuda, M., Anderson, J., Morgan, D.A., Mostoslavsky, R., Stuart, R.C., Perello, M., Vianna, C.R., Nillni, E.A., et al. (2010). SIRT1 deacetylase in POMC neurons is required for homeostatic defenses against diet-induced obesity. Cell Metab. *12*, 78–87.

Ramadori, G., Fujikawa, T., Anderson, J., Berglund, E.D., Frazao, R., Michán, S., Vianna, C.R., Sinclair, D.A., Elias, C.F., and Coppari, R. (2011). SIRT1 deacetylase in SF1 neurons protects against metabolic imbalance. Cell Metab. *14*, 301–312.

Ramadori, G., Konstantinidou, G., Venkateswaran, N., Biscotti, T., Morlock, L., Galié, M., Williams, N.S., Luchetti, M., Santinelli, A., Scaglioni, P.P., and Coppari, R. (2015). Diet-induced unresolved ER stress hinders KRAS-driven lung tumorigenesis. Cell Metab. *21*, 117–125.

Rodgers, J.T., Lerin, C., Haas, W., Gygi, S.P., Spiegelman, B.M., and Puigserver, P. (2005). Nutrient control of glucose homeostasis through a complex of PGC-1alpha and SIRT1. Nature *434*, 113–118.

Rubio-Sastre, P., Scheer, F.A., Gómez-Abellán, P., Madrid, J.A., and Garaulet, M. (2014). Acute melatonin administration in humans impairs glucose tolerance in both the morning and evening. Sleep (Basel) *37*, 1715–1719.

Saper, C.B., Scammell, T.E., and Lu, J. (2005). Hypothalamic regulation of sleep and circadian rhythms. Nature *437*, 1257–1263.

Scheer, F.A., Hilton, M.F., Mantzoros, C.S., and Shea, S.A. (2009). Adverse metabolic and cardiovascular consequences of circadian misalignment. Proc. Natl. Acad. Sci. U S A *106*, 4453–4458.

Service, F.J., Hall, L.D., Westland, R.E., O'Brien, P.C., Go, V.L., Haymond, M.W., and Rizza, R.A. (1983). Effects of size, time of day and sequence of meal ingestion on carbohydrate tolerance in normal subjects. Diabetologia *25*, 316–321.

Shi, S.Q., Ansari, T.S., McGuinness, O.P., Wasserman, D.H., and Johnson, C.H. (2013). Circadian disruption leads to insulin resistance and obesity. Curr. Biol. *23*, 372–381.

Shiuchi, T., Haque, M.S., Okamoto, S., Inoue, T., Kageyama, H., Lee, S., Toda, C., Suzuki, A., Bachman, E.S., Kim, Y.B., et al. (2009). Hypothalamic orexin stimulates feeding-associated glucose utilization in skeletal muscle via sympathetic nervous system. Cell Metab. *10*, 466–480.

Shiuchi, T., Toda, C., Okamoto, S., Coutinho, E.A., Saito, K., Miura, S., Ezaki, O., and Minokoshi, Y. (2017). Induction of glucose uptake in skeletal muscle by central leptin is mediated by muscle β_2-adrenergic receptor but not by AMPK. Sci. Rep. *7*, 15141.

Subramanian, A., Tamayo, P., Mootha, V.K., Mukherjee, S., Ebert, B.L., Gillette, M.A., Paulovich, A., Pomeroy, S.L., Golub, T.R., Lander, E.S., and Mesirov, J.P. (2005). Gene set enrichment analysis: a knowledge-based approach for interpreting genome-wide expression profiles. Proc. Natl. Acad. Sci. U S A *102*, 15545–15550.

Swinnen, S.G., Hoekstra, J.B., and DeVries, J.H. (2009). Insulin therapy for type 2 diabetes. Diabetes Care *32* (*Suppl 2*), S253–S259.

Takahashi, J.S. (2017). Transcriptional architecture of the mammalian circadian clock. Nat. Rev. Genet. *18*, 164–179.

Takahashi, J.S., Hong, H.K., Ko, C.H., and McDearmon, E.L. (2008). The genetics of mammalian circadian order and disorder: implications for physiology and disease. Nat. Rev. Genet. *9*, 764–775.

Talchai, C., Xuan, S., Lin, H.V., Sussel, L., and Accili, D. (2012). Pancreatic β cell dedifferentiation as a mechanism of diabetic β cell failure. Cell *150*, 1223–1234.

Toda, C., Shiuchi, T., Kageyama, H., Okamoto, S., Coutinho, E.A., Sato, T., Okamatsu-Ogura, Y., Yokota, S., Takagi, K., Tang, L., et al. (2013). Extracellular signal-regulated kinase in the ventromedial hypothalamus mediates leptin-induced glucose uptake in red-type skeletal muscle. Diabetes *62*, 2295–2307.

Todd, W.D., Fenselau, H., Wang, J.L., Zhang, R., Machado, N.L., Venner, A., Broadhurst, R.Y., Kaur, S., Lynagh, T., Olson, D.P., et al. (2018). A hypothalamic circuit for the circadian control of aggression. Nat. Neurosci. *21*, 717–724.

Trapnell, C., Roberts, A., Goff, L., Pertea, G., Kim, D., Kelley, D.R., Pimentel, H., Salzberg, S.L., Rinn, J.L., and Pachter, L. (2012). Differential gene and transcript expression analysis of RNA-seq experiments with TopHat and Cufflinks. Nat. Protoc. *7*, 562–578.

Umpierrez, G., and Korytkowski, M. (2016). Diabetic emergencies—ketoacidosis, hyperglycaemic hyperosmolar state and hypoglycaemia. Nat. Rev. Endocrinol. *12*, 222–232.

Van Cauter, E., Blackman, J.D., Roland, D., Spire, J.P., Refetoff, S., and Polonsky, K.S. (1991). Modulation of glucose regulation and insulin secretion by circadian rhythmicity and sleep. J. Clin. Invest. *88*, 934–942.

Versteeg, R.I., Stenvers, D.J., Visintainer, D., Linnenbank, A., Tanck, M.W., Zwanenburg, G., Smilde, A.K., Fliers, E., Kalsbeek, A., Serlie, M.J., et al. (2017). Acute effects of morning light on plasma glucose and triglycerides in healthy men and men with type 2 diabetes. J. Biol. Rhythms *32*, 130–142.

Vianna, C.R., and Coppari, R. (2011). A treasure trove of hypothalamic neurocircuitries governing body weight homeostasis. Endocrinology *152*, 11–18.

Wasserfall, C., Nick, H.S., Campbell-Thompson, M., Beachy, D., Haataja, L., Kusmartseva, I., Posgai, A., Beery, M., Rhodes, C., Bonifacio, E., et al. (2017). Persistence of pancreatic insulin mRNA expression and proinsulin protein in type 1 diabetes pancreata. Cell Metab. *26*, 568–575.e3.

Whichelow, M.J., Sturge, R.A., Keen, H., Jarrett, R.J., Stimmler, L., and Grainger, S. (1974). Diurnal variation in response to intravenous glucose. BMJ *1*, 488–491.

Yang, X., Downes, M., Yu, R.T., Bookout, A.L., He, W., Straume, M., Mangelsdorf, D.J., and Evans, R.M. (2006). Nuclear receptor expression links the circadian clock to metabolism. Cell *126*, 801–810.

Zhang, E.E., and Kay, S.A. (2010). Clocks not winding down: unravelling circadian networks. Nat. Rev. Mol. Cell Biol. *11*, 764–776.

STAR★METHODS

KEY RESOURCES TABLE

REAGENT or RESOURCE	SOURCE	IDENTIFIER
Antibodies		
Phospho-Akt (Thr308)	Cell Signaling Technology	Cat# 4056, RRID:AB_331163
Akt	Cell Signaling Technology	Cat# 2920, RRID:AB_1147620
SIRT1	Merck	Cat# 07-131, RRID:AB_2188349
pADRB2 (Ser355/Ser356)	Thermo Fisher Scientific	Cat# PA5-38403, RRID:AB_2555004
ADRB2	Thermo Fisher Scientific	Cat# PA5-14117, RRID:AB_2225403
GAPDH	Cell Signaling Technology	Cat# 5014, RRID:AB_10693448
GSK-3β	Cell Signaling Technology	Cat# 9315, RRID:AB_490890
pGSK-3β	Cell Signaling Technology	Cat# 9336, RRID:AB_331405
BMAL1	Abcam	Cat# ab93806, RRID:AB_10675117
PGC-1α	Santa Cruz	Cat# sc-13067, RRID:AB_2166218
Critical Commercial Assays		
Avidin Biotin Complex	Vector Laboratories	PK-6100
Mouse Insulin ELISA Kit	Crystal Chem. Inc.	90080
Deposited Data		
Transcriptomics data	this paper	GEO:GSE129518
Experimental Models: Organisms/Strains		
Sf1-Cre; *Sirt1*$^{loxP/loxP}$	This paper	Ramadori et al., 2011
Sirt1$^{loxP/loxP}$	This paper	Ramadori et al., 2011
Sf1-Cre; *Bmal1*$^{loxP/loxP}$	This paper	Orozco-Solis et al., 2016
Bmal1$^{loxP/loxP}$	This paper	Orozco-Solis et al., 2016
Software and Algorithms		
Microsoft Office Excel 2010	Microsoft	https://www.microsoft.com
GraphPad	GraphPad Software Inc	https://www.graphpad.com

CONTACT FOR REAGENT AND RESOURCE SHARING

Further information and requests for resources and reagents should be directed and will be fulfilled by the Lead Contact, Roberto Coppari (Roberto.coppari@unige.ch).

EXPERIMENTAL MODEL AND SUBJECT DETAILS

Sf1-Cre; *Sirt1*$^{loxP/loxP}$ and *Sirt1*$^{loxP/loxP}$ mice were housed at the animal facilities of University of Geneva, in accordance with the animal care and experimentation authorities of the Canton of Geneva, Switzerland (animal protocol numbers GE/22/15, GE/28/13, GE/120/15). *Sf1*-Cre; *Bmal1*$^{loxP/loxP}$ and *Bmal1*$^{loxP/loxP}$ mice were housed at the animal facilities of the University of California, Irvine. Animals and protocols used in this study were reviewed and approved by the Institutional Animal Care and Use Committee of the University of California, Irvine.

METHODS DETAILS

Animal Experiments

Sf1-Cre; *Sirt1*$^{loxP/loxP}$ and control (*Sirt1*$^{loxP/loxP}$) mice were housed in groups of 4-5 with a standard chow rodent diet and water available *ad libitum* in light- and temperature-controlled environments unless otherwise specified. LD mice were exposed to 12-hour light and 12-hour dark cycles. They were sacrificed and tissues were collected every 6 hours. DD mice were exposed to darkness for 30 days. They were sacrificed subsequently around the clock every 4 hours. LDL mice were exposed to 12-hour light, 5-hour dark, 1-hour light, and 6-hour dark cycles for 30 days with applied light stimulus was 400 lux (incandescent light) (Ishida et al.,

2005). After the end of 30 days, they were sacrificed subsequently around the clock every 4 hours. For the insulin-stimulated experiments, 2DD mice were exposed to darkness for 2 days. To avoid post-prandial confounding effects, insulin or saline administration was performed in mice that had no access to food starting 3 hours prior to injection; yet, water was available *ad libitum*. For *in vivo* insulin-induced glucose uptake experiments, animals were exposed to darkness for 2 days (2DD) of light in the middle of night for 30 days (LDL). *in vivo* insulin-stimulated glucose uptake in tissues was performed at ZT6 and determined by a 40 μCi bolus injection of 2-deoxy-[1,2-^{3}H]-glucose (ARC, St-Louis, MO) i.v. in the presence of insulin (Humulin, Lilly France) at 0.75 IU/kg i.p. Blood was sampled from the tail vein 1, 7, 14, 21 and 28 minutes after injections. After 30 minutes, mice were rapidly sacrificed and tissues removed and stored at −80°C until use. Glucose concentration in deproteinized blood samples was measured using the glucose oxidase method (GLU, Roche Diagnostics, Rotkreuz, Switzerland). Measurements of [1,2-^{3}H] deoxyglucose-6-phosphate levels in deproteinized blood samples and individual tissues allowed calculation of the glucose utilization index in tissues. *Sf1*-Cre; *Bmal1*$^{loxP/loxP}$ and control (*Bmal1*$^{loxP/loxP}$) mice were maintained on a 12-hour light/dark cycle. Tissues were immediately flash frozen in liquid nitrogen for subsequent processing.

Circadian Behavior

Wheel-running activity was continuously recorded and data was obtained every 5 min using Columbus Instruments Multi-Device Instruments (Columbus, OH, USA). Data were analyzed using ActogramJ (NIH).

Real-Time Quantitative Polymerase Chain Reaction (Real-Time qPCR)

RNAs were extracted using Trizol reagent (Invitrogen). Complementary DNA was generated by Superscript II (Invitrogen) and used with SYBR Green PCR master mix (Applied Biosystem, Foster City, CA, USA) for quantitative real time PCR (q-RTPCR) analysis. mRNA contents were normalized to *18 s* mRNA levels. All assays were performed using an Applied Biosystems QuantStudio® 5 Real-Time PCR System. For each mRNA assessment, q-RTPCR analyses were repeated at least 3 times.

Western Blot

Proteins were extracted by homogenizing samples in lysis buffer (Tris 20mM, EDTA 5mM, NP40 1% (v/v), protease inhibitors (P2714-1BTL from Sigma, St. Louis, MO, USA). Generally, 30 μg of tissues was loaded on 10% poly-acrylamide gels and finally transferred to a nitrocellulose membrane by electroblotting. Briefly, nitrocellulose membranes were blocked with Odyssey blocking buffer (Li-Cor Biosciences) 1 hour at room temperature and successively incubated 12 hours at 4°C with the specific primary antibodies diluted 1:1000 in PBS-T buffer. PBS-T buffer is PBS buffer (27.6g Sodium Phosphate, dibasic + 160 g Sodium Chloride in 20L distilled H_2O at pH 7.4) and 0.5% Tween-20. Detection was obtained by using near-infrared secondary antibodies diluted 1:5000 in PBS-T (IRDye 800CW and IRDye600RD; Li-Cor Biosciences) and a Clx Odyssey infrared scanner (Li-Cor Biosciences). List of antibodies used for western blotting are as follows: pAKT - Phospho-Akt (Thr308) (244F9) (Rabbit Ab, Cell Signaling Technology), AKT - Akt (pan) (40D4) (Mouse mAb, Cell Signaling Technology), GSK-3β (D5C5Z) (XP® Rabbit Ab, Cell Signaling Technology), Phospho-GSK-3β (Ser9) (Cell Signaling Technology), BMAL1 (Abcam Ab93806), PGC-1α (H-300) (sc-13067, Santa Cruz), GAPDH (14C10) (Rabbit Ab, Cell Signaling Technology), Phospho-beta-2 Adrenergic Receptor (Ser355/Ser356) (PA5-38403) (Rabbit Ab, Thermo Fisher Scientific), Beta-2 Adrenergic Receptor (PA5-14117) (Rabbit Ab, Thermo Fisher Scientific).

Blood Chemistry

Fed hormones/metabolites levels were determined by collecting tail blood from mice that were without food for 3 hours. Fasted hormones/metabolites levels were assessed in mice provided only with water *ad libitum* and without food for the indicated period. Time at day at which blood was collected was the same between groups. Tail vein blood was assayed for glucose levels using a standard glucometer (Nova Biomedical). Plasma was collected by centrifugation in EDTA-coated tubes (Kent Scientific) and assayed for insulin (Crystal Chem. Inc.) levels using the indicated commercially available kit.

Immunohistochemistry Analyses

Nissl staining and SIRT1 immunohistochemistry were performed using free-floating brain sections as previously described (Ramadori et al., 2010). Briefly, 25 μm thick sections were mounted on glass slides and treated in xylene and then PBS containing decreasing concentration of ethanol (100%, 70%, 50% and 0%). All steps were performed at room temperature on an orbital shaker at ~50 rpm. Sections stored in PBS were first washed in PBS 3 times for 10 minutes each. Sections were then incubated in 0.3% H_2O_2 for 30 minutes to block the endogenous peroxidase activity and subsequently rinsed in PBS 3 times for 10 minutes each. All sections were then placed in blocking solution of 3% normal donkey serum in PBT-Azide (2.5mL of Triton X-100 in 1000mL of PBS-Azide) for 2 hours. The sections were then transferred into SIRT1 1:5,000 primary antisera (Anti-Sir2 Antibody 07-131, Merck) with 3% normal donkey serum in PBT-Azide overnight at 4°C. The sections were then rinsed with PBS 6 times for 10 minutes each. Next, sections were transferred into 1:1,000 biotin-conjugated donkey anti-rabbit secondary antisera (Jackson Immuno Research) with 3% normal donkey serum in PBT for 2 hours and subsequently rinsed in PBS 3 times for 10 minutes each. Avidin Biotin Complex (Vectastain Elite PK-6100 ABC kit, Vector Laboratories) solution was prepared (1:500 in PBS) 30 minutes prior to incubating the sections in it for 1 hour and subsequently rinsed in PBS 2 times for 10 minutes each. The sections were then incubated in 0.04%

3,3′-Diaminobenzidine and 0.01% H_2O_2 in PBS for 8 minutes. Finally, the sections were washed in PBS 2 times for 10 minutes each and mounted on gelatin coated glass slides for visualization. Adjacent sections were used for Nills staining.

RNA sequencing and analysis

RNA sequencing

Total RNA was extracted at from skeletal muscle using methods previously described in preparation for RNA sequencing (RNASeq). Quality control was done using the Agilent Bioanalyzer Nano RNA chip and Nanodrop. Library construction was performed according to the Illumina TruSeq mRNA stranded protocol. In total, 32 samples corresponding to 4 ZTs (ZT0, 6, 12, and 18) were multiplexed into 4 libraries of 8 samples for both genotypes, and sequenced on an Illumina HiSeq 2500 instrument during two single-end 100 cycles sequencing runs by the Genomics High-Throughput Facility at the University of California, Irvine. The resulting sequencing data for each library were post-processed and demultiplexed to produce FastQ files using Illumina software CASAVA. Reads failing Illumina's standard quality tests were not included in the FastQ files. The quality of the remaining sequences was further assessed using the PHRED quality scores produced in real time during the base-calling step of the sequencing runs. Filtered FastQ files were then processed through the standard Tuxedo protocol (Trapnell et al., 2012). Briefly, reads were aligned to the UCSC mm10 mouse reference genome using TopHat and Bowtie2 with standard recommended parameters. Assembled transcripts were obtained via Cufflinks with the mm10 reference annotation file. Genome assembly was obtained using Cuffmerge and expression levels (summarized to genes) were calculated using Cuffquant and then normalized via Cuffnorm to FPKM values. For each condition, 24 hr. time series data from 4 time points with 4-5 replicates each was collected. In total, expression levels of 24138 unique genes were considered for further analysis. Data was further organized into two parallel circadian groups (one per condition) for comparative analysis.

Circadian Analysis

Gene expressions with low or sparse FPKM values (< 0.1 in at least half of the samples) were filtered, resulting in 16634 high quality data rows for downstream analysis. Time series of expression levels were then used to determine circadian behaviors of transcripts using BIO_CYCLE algorithm (Agostinelli et al., 2016) a modern circadian oscillation predicting method based on a neural network approach, and corroborated using JTK-CYCLE (Hughes et al., 2010). A time series with $p < 0.05$ was considered significantly rhythmic over the circadian cycle. False discovery rates were estimated using the Benjamini-Hochberg q (BHQ) values. Amplitude, phase and period predicted by BIO_CYCLE was generated for all gene expressions passing this threshold. Distributions of phase and amplitude of circadian genes were analyzed done using 'sci-kit learn' and 'pandas' in python. Amplitude distribution of oscillating genes was analyzed by Mann-Whitney test. Evaluation of phase lag between conditions was carried out by Wilcoxon Signed Rank Test where a phase difference of 1 hour or more was considered a phase change. Heatmaps of the rhythmic expressions were generated by R package 'gplots'.

Statistical and Bioinformatics Analysis

Differential analysis of expression levels between the conditions at a specific ZTs was done using Cyber-T (Kayala and Baldi, 2012), a differential analysis program using a Bayesian-regularized t test. Fold change (FC) was calculated with FPKM values. An enrichment analysis based on the Gene Set Enrichment Analysis methodology was used to discover potentially enriched pathways and upstream transcription factors or RNA-binding proteins (Subramanian et al., 2005). For pathway information, gene ontological data from PathwayCommons was used, for TFs information predicted binding sites from MotifMap and MotifMap-RNA were used (Cerami et al., 2011; Liu et al., 2017). Gene sets with FDR < 0.05 were considered significantly enriched and were ranked using fold changes or the number of genes in the set. Most of the aforementioned analysis was done using pipelines implemented for the CircadiOmics (Patel et al., 2012) database and web portal (http://circadiomics.ics.uci.edu) where all the transcriptomic data associated with this work is publicly available on database link "MOUSE SKELETAL MUSCLE NA 2018."

QUANTIFICATION AND STATISTICAL ANALYSIS

Quantification

Western blots for pan acetylated lysine antibody were quantified using ImageJ (NIH).

Statistical Analysis

Datasets were analyzed for statistical significance using PRISM (GraphPad, San Diego, CA) for a two-tail unpaired Student's t test when two groups were compared or one-or two-way ANOVA (Tukey's post-test) when more than two groups were compared.

DATA AND SOFTWARE AVAILABILITY

The accession number for the data reported in this paper is GEO: GSE129518 (Database: https://www.ncbi.nlm.nih.gov/geo/query/acc.cgi?acc=GSE129518).